Top Curr Chem (2014) 347: 303–346
DOI: 10.1007/128_2014_530

Published online: 20 May 2014

Dynamical Mean Field Theory-Based Electronic Structure Calculations for Correlated Materials

Silke Biermann

Abstract We give an introduction to dynamical mean field approaches to *correlated materials*. Starting from the concept of electronic correlation, we explain why a theoretical description of correlations in spectroscopic properties needs to go beyond the single-particle picture of band theory.

We discuss the main ideas of dynamical mean field theory and its use within realistic electronic structure calculations, illustrated by examples of transition metals, transition metal oxides, and rare-earth compounds. Finally, we summarise recent progress on the calculation of effective Hubbard interactions and the description of dynamical screening effects in solids.

Keywords Electronic Correlations · Correlated Materials · Dynamical Mean Field Theory · Density Functional Theory and Beyond · Constrained Random Phase Approximation · Transition Metals · Transition Metal Oxides · Rare Earth Pigments · Dynamical Screening in Solids

Contents

S. Biermann (✉)
Centre de Physique Théorique, Ecole Polytechnique, CNRS UMR7644, Palaiseau 91128, France
e-mail: biermann@cpht.polytechnique.fr

1 Overview

This chapter gives an introduction to theoretical approaches to spectroscopic properties of *correlated materials*, with an emphasis on dynamical mean field-based methods. We start with a brief introduction to electronic correlations, from their definition and experimental signatures to the tremendous challenges they pose to a theoretical description. We explain why a theoretical description of correlations in spectroscopic properties cannot be obtained within the single-particle picture of band theory, and how to resolve the apparent contradiction that *ground state energies* calculated from density functional theory (DFT) nevertheless contain a correlation contribution. We then identify the competition between the two counteracting tendencies of electrons to localise due to Coulomb interactions and to delocalise in order to lower their kinetic energy as the key ingredient determining correlated electron behaviour. The Hubbard model, as the simplest theoretical model describing this balance, is introduced, and its dynamical mean field solution is discussed. We describe the main ideas of dynamical mean field theory (DMFT), give the equations in the Hubbard model case and discuss the generalisation to realistic electronic structure calculations, in the form of the combined DFT + DMFT scheme. Three examples to illustrate the power of the method are chosen among calculations for the most representative classes of compounds: transition metals, transition metal oxides and rare-earth compounds. We summarise further aspects of DFT + DMFT schemes, concerning their theoretical foundations, technical aspects and extensions. Then we present recent developments in the field, extending the combined DFT + DMFT scheme to include dynamically screened Coulomb interactions. Finally, we summarise recent advances in combined GW + DMFT calculations, where the DFT starting point is replaced by many-body perturbation theory within Hedin's formulation. We conclude this chapter by discussing open questions and further perspectives in the field.

2 Band Theory as a Low-Energy Description: The Miracle of Screening and Quasi-Particles

The mission of solid state physics is, quite generally, to relate macroscopic properties of solids, such as electrical or thermal conductivities, spectroscopic or optical properties, thermodynamical behaviour or magnetic phenomena, to the microscopic behaviour of their constituents, ions and electrons. Progress in physics within the twentieth century provided the two ingredients that are instrumental for this enterprise: quantum mechanics and statistical physics.

The application of the newly developed quantum theory to electronic states in periodic potentials by Felix Bloch, in his Ph.D. thesis entitled "Über die Quantenmechanik der Elektronen in Kristallgittern" in 1928, can be considered the foundation of modern solid state physics. It led to the development of band theory, which establishes the form of the eigenstates of an electron in a periodic potential, characterised by – apart from spin – two quantum numbers, the quasi-momentum vector $\mathbf{k}$ of the electron in the solid and a band index. The corresponding eigenstates form continuous (as a function of $\mathbf{k}$) energy bands, forming what is commonly known as the "band structure" of the solid. Bloch's theory then assumes an "independent electron picture" to be valid, where the band states are filled respecting the Pauli principle. This amounts to postulating that any effects of the Coulomb interactions between the electrons can be cast into an effective one-body potential. Hartree, Hartree–Fock, or, later on, DFT provide explicit constructions for such potentials (and the Hohenberg–Kohn theorem, remarkably, states that, for the purpose of only calculating ground state properties, this assumption can in fact be made rigorous).

Experimental techniques such as angle-resolved photoemission spectroscopy (ARPES) are nowadays able to map out explicitly band structures of solids, and the agreement with theoretical predictions is often surprisingly good for simple solids, see, e.g. the example of copper in [1] (Fig. 24 therein). For somewhat less simple solids, e.g. transition metals or certain classes of oxides, corrections become necessary, but it is remarkable that the band picture as such often survives. When naively estimating orders of magnitude of different energetic contributions, this may come as a surprise: in fact, when estimating the matrix element of the electronic Coulomb interaction between 3d-orbitals of nickel, for example, the resulting value of 25 eV [2, 3] exceeds the bandwidth of this material by an order of magnitude, and one would naively believe that a theory that makes the most drastic approximation on the largest – the interaction – term should not be meaningful. It can be considered as one of the miracles of solid state physics that it is. The reasons are subtle: first of all, *screening* of the interactions in the solid reduces the Coulomb interactions by an order of magnitude so that the relevant energy scale is not an interaction of 25 eV but rather of 2–3 eV. More importantly, however, Landau's theory of quasi-particles teaches us that the band picture may survive as a low-energy effective theory close to the Fermi level, where Coulomb interactions renormalise away (in a renormalisation group sense) as a consequence

of the Pauli principle and resulting phase space arguments. This is consistent with ARPES findings on a large variety of materials where quasi-particle bands are observed, but undergo more or less severe renormalisation effects, corresponding to enhancements of the mass of the quasi-particles (see, e.g. [4]). The reduction of the spectral weight contained in the quasi-particle features of a spectrum is necessarily accompanied with spectral weight transfers towards higher energy satellite features, lying beyond the window of the validity of a low-energy effective theory and thus not contained in band theory. Another important consequence is an intrinsic temperature dependence of the electronic structure: in Bloch's band theory, temperature dependence enters only through the Fermi factor determining the occupation of one-particle states, whereas Landau theory teaches us that the validity of the low-energy theory (and this means in fact the band picture) is itself temperature-dependent. Fermi liquids are characterised by a temperature ("coherence") scale above which the quasi-particle picture ceases to be valid.[1] It adds to the thrill of exploring correlated electron physics that this scale can vary from a fraction of a Kelvin in heavy fermion compounds to several hundreds or even thousands of Kelvin in weakly correlated materials.

In cases where screening is not efficient enough to reduce the effective Coulomb interactions and the Fermi liquid solution is no longer a stable fixed point of the low-energy theory, entirely new phenomena, far beyond band theory, occur [6]. The simplest is the Mott insulating phase where interaction effects lead to localised electron behaviour: the interaction energy cost associated with the multiple occupancy of an atomic site overcompensates for any possible gain in electron kinetic energy that would result from delocalisation. This state is characterised by insulating behaviour for any commensurate electron filling.

The situation becomes more complicated when additional symmetry breaking occurs, and ordering phenomena involving spin, charge or orbital degrees of freedom and their coupling come into play. Frustration potentially enhances quantum fluctuations and can lead to emergent exotic orders around quantum critical points. Electron–electron interactions are also the source of unconventional superconductivity, metal–insulator transitions, or giant responses to tiny perturbations – phenomena with tremendous potential for applications. We cite as an example the metal–insulator transition and the corresponding thermochromic properties of vanadium dioxide, motivating its use as "intelligent" window coatings [7–10].

[1] For a review of the Mott transition comprising a discussion of coherence–decoherence crossovers see, e.g. [5].

3 Correlations

The word "correlation" stems from the Latin word "correlatio" meaning mutual relationship, and designates an interdependence of the behaviour of two or more constituents of a system. In mathematical terms, two statistical quantities A and B are correlated, if the average of the product AB differs from the product of their averages:

$$\langle AB \rangle \neq \langle A \rangle \langle B \rangle . \tag{1}$$

On this basis, the term "correlation" is used in various areas of social and natural sciences.

The obvious quantum mechanical generalisation of the term amounts to defining two observables as correlated if the associated operators, A, B, obey the above inequality where the statistical average is replaced by the quantum mechanical expectation value. At finite temperatures, both quantum mechanical expectation value and thermodynamical average are implied.

For quite obvious reasons, electronic correlations are intimately linked to the electronic Coulomb interactions. First, it is the two-body nature of the Coulomb interaction operator that induces electronic correlations, and any non-interacting theory leads to uncorrelated electronic behaviour, involving independent electrons described by a Slater determinant. Conversely, if electrons behave in a correlated way, this immediately leads to an energetic contribution stemming from Coulomb interactions beyond the mean field energy. This is easily seen in the simple example of a single atomic orbital, the occupation of which is measured by the observables $n_\uparrow$ and $n_\downarrow$ that count, respectively, the numbers of electrons with spins up and down in this orbital. Correlated behaviour is then equivalent to a non-vanishing difference $\langle n_\uparrow n_\downarrow \rangle - \langle n_\uparrow \rangle \langle n_\downarrow \rangle$, and the Coulomb interaction energy is composed of two terms: the mean field contribution (Hartree term) $U \langle n_\uparrow \rangle \langle n_\downarrow \rangle$ and the correlation energy U $(\langle n_\uparrow n_\downarrow \rangle - \langle n_\uparrow \rangle \langle n_\downarrow \rangle)$, where U denotes the matrix element of the Coulomb operator v in the wave function corresponding to the atomic orbital: $U = \langle \phi\phi | v | \phi\phi \rangle$.

For electronic states that are Slater determinants of one-particle eigenstates of a separable Hamiltonian,[2] expectation values of two-particle operators factorise, and their behaviour is thus uncorrelated. This specifically is the case with the band picture of Bloch theory. Many-body effects, that is, correlations resulting in a suppression of the double occupancy compared to its uncorrelated value, $\langle n_\uparrow n_\downarrow \rangle < \langle n_\uparrow \rangle \langle n_\downarrow \rangle$, are thus always effects *beyond* the band picture.[3] This is true independently of how the bands are calculated, that is, which effective potential was used as

[2] A many-body Hamiltonian is called separable if it can be written as a sum over operators each acting only on one electron.

[3] Even though it is of course always possible to design an auxiliary one-particle system for the purpose of *parametrising* certain physical quantities, such as the density, as done in the Kohn-Sham construction of density functional theory.

an approximation to the Coulomb interactions (the Hartree potential, or the Kohn–Sham potential of density functional theory, or any other choice).

A particularly interesting case is that of a paramagnetic Mott insulator, i.e. a phase where the double occupancy is largely suppressed, $\langle n_\uparrow n_\downarrow \rangle \sim 0$, while the density per orbital and spin $\langle n_\uparrow \rangle = \langle n_\downarrow \rangle$ takes a finite value corresponding to the density of the system. This situation is realised in the strong coupling limit, i.e. when the Coulomb interaction U is the dominant energy scale in the system, outweighing any possible gain in kinetic energy due to delocalisation of the electrons. In nature, the ground state of correlated insulators such as transition metal oxides is usually an ordered phase[4] and the paramagnetic state is realised only above a certain ordering temperature. A subtle question then arises from the fact that in a broken-symmetry phase it is possible to open an insulating gap without the need for correlations in the strict sense. Indeed, a state with vanishing double occupancy $\langle n_\uparrow n_\downarrow \rangle \sim 0$ is readily realised even in the independent particle picture if for each atomic orbital one of the two spin occupations, $\langle n_\uparrow \rangle$ or $\langle n_\downarrow \rangle$, vanishes. This is trivially the case in a ferromagnetic or antiferromagnetic material with full polarisation.

This observation explains the success of LDA + U-derived methods [11], hybrid functionals, the quasi-particle GW approximation and other schemes geared to calculating one-particle band structures in opening band gaps in magnetic or charge-ordered materials. It does not imply, however, that these techniques are appropriate for describing spectra of Mott insulating states originating from electronic correlations in the many-body sense. Here and in the following we define many-body correlations as effects that result from a non-vanishing correlator $\langle n_\uparrow n_\downarrow \rangle - \langle n_\uparrow \rangle \langle n_\downarrow \rangle$, which, as argued above, cannot be realised within *any* band theory or one-particle description.

Physically, this inadequacy is easily seen from a comparison of the relevant energy scales: a material such as Ce_2O_3 displays a gap of several eV (corresponding to a temperature scale of several 10^4 K) but has a Néel temperature below 10 K. This mismatch demonstrates that the magnetic order is not the primary cause for the insulating nature. Mott localisation and local moment formation are consequences of the many-body interactions, and happen independently of the ordering of local moments at low temperatures. Even though the ordered state can itself often be cast into a one-particle band picture, electronic structure techniques that rely on the magnetism for opening the gap should not be expected to describe other aspects of the many-body physics of such compounds. An important goal for techniques beyond LDA or LDA + U therefore includes the *finite temperature* description of materials. That the temperature dependence of their electronic properties is not restricted to effects that can be traced back to occupations varying according to a Fermi factor is precisely one of the most striking hallmarks of correlated materials [12].

[4] We do not enter here into the subtle questions of frustrations leading to possible spin liquid phases.

4 Density Functional Theory

The reader familiar with density functional theory will likely now wonder how to reconcile the above with the Hohenberg–Kohn theorem and the Kohn–Sham construction [13–15]. Indeed, the Hohenberg–Kohn theorem teaches us that ground state properties of an electron gas in an external potential are functionals of the density $\rho(\mathbf{r})$ alone. In particular, there exists a functional $E(\rho)$ such that minimisation of this functional allows for the determination of the ground state energy and density: $E_{\mathrm{gs}} = E[\rho_{\mathrm{gs}}] = \min E[\rho]$. A formal expression for the energy functional

$$E[\rho] = T_0[\rho] + \int \mathrm{d}\mathbf{r}\rho(\mathbf{r})\left(v_{\mathrm{ext}}(\mathbf{r}) + \frac{1}{2}v_{\mathrm{H}}(\mathbf{r})\right) + E_{\mathrm{xc}}[\rho] \tag{2}$$

contains as one-body terms the kinetic energy T_0 of an auxiliary (non-interacting) Kohn–Sham system of density $\rho(\mathbf{r})$, the energy associated with the external potential v_{ext}, the Hartree potential v_{H} and the – non-trivial – exchange-correlation energy E_{xc}. Even though this term enters in the form of an auxiliary additional one-body potential $\nu_{\mathrm{xc}} = \frac{\delta E_{\mathrm{xc}}}{\delta\rho}$ in the Kohn–Sham construction, it is clear that it contains in fact the many-body correlations of the system. A purely formal but instructive exact expression can be derived by coupling-constant integration:

$$E_{\mathrm{xc}} = \frac{1}{2}\int\int \mathrm{d}\mathbf{r}\,\mathrm{d}\mathbf{r}'\,\frac{n(\mathbf{r})n_{\mathrm{xc}}(\mathbf{r}-\mathbf{r}',\mathbf{r}')}{|\mathbf{r}-\mathbf{r}'|} \tag{3}$$

with the exchange-correlation hole defined as

$$n_{\mathrm{xc}}(\mathbf{r}-\mathbf{r}',\mathbf{r}') = n(\mathbf{r}')\int_0^1 \mathrm{d}\lambda(g(\mathbf{r},\mathbf{r}',\lambda)-1). \tag{4}$$

Here, $g(\mathbf{r},\mathbf{r}',\lambda)$ denotes the pair correlation function of an interacting electron gas of density ρ where the Coulomb interaction has been scaled by λ (that is, for $\lambda = 0$ one recovers the Kohn–Sham system and for $\lambda = 1$ the true Coulomb system is obtained). The "exchange-correlation hole" n_{xc} describes the depletion in electronic density at point $\mathbf{r}'$ due to the presence of an electron at point $\mathbf{r}$. The exchange-correlation energy corresponds to the energy gain due to the interaction of the electronic density with this effective positive depletion charge, the exchange-correlation hole.

The reader will have recognised that this is precisely the effect described before within the simple one-orbital model where the correlator $\langle n_\uparrow n_\downarrow\rangle - \langle n_\uparrow\rangle\langle n_\downarrow\rangle$ describes the suppression of the probability of finding a second electron given the

presence of a first one. The associated reduction in Coulomb energy is the correlation energy discussed before.[5]

Let us stress an important point emerging from the discussion above: while the total energy of DFT contains, of course, the energetic contributions of the full many-body physics (this statement is obvious, since the energy obtained from the exact Hohenberg–Kohn functional would be exact!), the mapping onto the auxiliary Kohn–Sham system corresponds to replacing the many-body problem by a single-particle one. Therefore, no physical quantity derived from the Kohn–Sham system, other than ground state quantities such as the total energy and the density, contains many-body correlations. This is in particular true for the eigenvalues derived from the auxiliary non-interacting system, the Kohn–Sham band structure. Nevertheless, the well-known success of the comparison of Kohn–Sham band structures to ARPES spectra for simple metals teaches us that, if the Fermi liquid picture is applicable, that is, if a band structure exists, the one-particle potential given by Kohn–Sham theory is a much better approximation to the true spectrum than, e.g. the Hartree–Fock one.

An important corollary of the above discussion is that the strength of many-body correlations, or the importance of corrections to the one-particle picture, crucially depends on the quantity considered. If we define correlations as effects beyond *the best possible* one-particle picture, Hohenberg–Kohn theory would indicate that there are *no correlations* in the total energy of an electron gas, even in its Mott insulating phase! Indeed, for the purpose of calculating total energies, the best one-particle picture is precisely the Kohn–Sham band structure corresponding to the exact density functional, and the corresponding energy is the exact ground state energy. This does not mean, however, that spectral properties of Mott insulators are accessible within a band picture. Yet another instructive example will be simple semiconductors such as silicon where clearly the one-particle spectrum is well-described within the band picture. Still, this success of one-particle theory does not imply that, for example, plasmon excitations would be contained in a single-particle description.

Yet another point becomes obvious from the above reasoning; namely, the importance of defining the reference one-particle picture with respect to which corrections are considered. When following the definition of correlations of standard textbooks on solid state physics, e.g. Ashcroft and Mermin, one would take the Hartree–Fock picture as a reference single-particle theory. Modern many-body theories, in contrast, often work out corrections to the Kohn–Sham band structure of DFT. We have alluded above to the concept of a "best single-particle" picture. The philosophy of the latter is that any corrections that take on the form of a static potential can readily be absorbed into the one-particle description. Correlation effects are then purely described by a many-body self-energy, and it is in fact the frequency-dependence of the latter that encodes the many-body correlations. In this

[5] Due to the presence of only two electrons, with different spins, the simple one-orbital model did not involve any effects of electronic exchange.

respect, we note that different one-particle starting points differ by definition only by static one-body potentials, and thus the ambiguity induced in practise by the choice of the respective reference system does not constitute a conceptual limitation.[6]

Accordingly, when discussing effects "beyond band theory" in this chapter, we will be referring to the single-particle picture in a generic way, without conceptual reference to a specific choice of a band structure method. In particular, the "failures of band theory" that we will discuss below are not to be interpreted as inadequacies of the Kohn–Sham band structure, but true breakdowns of the single-particle picture as such *independently of the specific choice of band picture*. This is not in contradiction with the fact that, in practice, most first-principles many-body calculations use the Kohn-Sham band structure of DFT-LDA as a starting point for a many-body treatment.

5 The Hubbard Model

It is one of the virtues of the elegant construction of DFT to include the correlation contribution to the ground state energy, without dealing with it explicitly. Somewhat surprisingly, the homogeneous electron gas turned out to be a powerful reference system from which accurate and efficient approximations such as the local density approximation or generalised gradient schemes have been obtained. At the same time, the many-body wave function of electrons in a solid with partially filled *d*- or *f*-shells has probably little in common with the eigenstates of the homogeneous electron gas, let alone with a Slater determinant of Kohn–Sham one-particle wave functions. Spectroscopic probes of transition metal oxides or rare earth or actinide systems rather found indications of the usefulness of an entirely different starting point for the description of experimental findings: the isolated atom.

The correlation problem as evidenced from spectral properties of materials is indeed intimately related to the trivial observation that solids are made of atoms, and that some of the atomic behaviour survives in the solid state. We connect to a simple argument due to Mott [17] meant to demonstrate the limitations of the band description and to illustrate nicely the relation to the atomic picture. Consider a collection of atoms with a single valence electron and a single orbital, e.g. hydrogen, and let us forget for the moment their tendency to molecule formation. Arranging the atoms in a periodic structure with one atom per unit cell and a lattice constant of the order of Ångstroms results – according to Bloch's theorem –

[6] This also means that we are not entering into an exhaustive discussion of what should be the "best" starting one-body picture to build DMFT on. The section on GW + DMFT contains some implicit information on this issue, but systematic comparisons have not been performed so far (see however the discussion in [16]).

in a half-filled band and thus in a metallic state. The physical mechanism behind the band formation is the kinetic energy gain associated with the delocalisation of the electrons. Now consider the following *Gedankenexperiment*: let us increase the lattice constant to artificially large values, such as to decrease the kinetic energy gain and, in particular, to make it smaller than the price of the Coulomb interaction that we have to pay when two electrons occupy the same atom. Band theory would still postulate the system to be conducting, independently of the value of the interatomic distances – "against common experience and, one might say, common sense", as Mott put it [17]. In reality, in this situation hopping becomes unfavourable, and the ground state consists of electrons being localised on their respective atoms. The system is just reduced to a collection of independent atoms. In other words, in this "atomic limit" the ground state is *not* the Slater determinant of Bloch states postulated by Bloch's theorem.[7] It is the competition with the Coulomb interaction associated with double occupancies that destroys the Bloch state. In fact, in this situation it is more appropriate to think in terms of real space, in an atomic picture, rather than in k-space. To first approximation, we can entirely neglect the kinetic energy and write the effective Hamiltonian for the Coulomb interactions:

$$H_{\text{int}} = \sum_i U n_{i\uparrow} n_{i\downarrow}. \tag{5}$$

Here, $n_{i\sigma}$ are the occupation number operators corresponding to electrons in the s-orbital on site i with spin σ; they commute with the Hamiltonian and are thus good quantum numbers. The Hamiltonian is thus diagonal in the eigenbasis of these operators, and the eigenstates can simply be labelled by these atomic occupation numbers. We are thus naturally led to a real-space picture. This is in contrast to the kinetic energy part of the Hamiltonian[8]

$$H_{\text{kin}} = \sum_{ij\sigma} t_{ij} c^\dagger_{i\sigma} c_{j\sigma}, \tag{6}$$

which is diagonal in momentum space. Indeed, Fourier transformation of the creation and annihilation operators for an electron at site i and with spin σ, $c^\dagger_{i\sigma}$ and $c_{j\sigma}$ according to standard rules diagonalises the Hamiltonian:

$$H_{\text{kin}} = \sum_{k\sigma} \varepsilon_k c^\dagger_{k\sigma} c_{k\sigma}, \tag{7}$$

with

[7] And not even a Slater determinant.

[8] This part can in fact be thought of as comprising, apart from the kinetic energy, any one-body potential, e.g. the electrostatic potential created by the ions.

$$\epsilon_k = \sum_{ij} t_{ij} e^{ik\left(R_i - R_j\right)}. \tag{8}$$

Here, R_n denote the lattice sites, and the k-vectors are the crystal momenta as in Bloch's theorem.

Despite its simplicity, the above example illustrates the physical mechanisms at work in systems that require a description beyond one-particle approaches. Indeed, in between the two limits – the band picture of non-interacting Bloch electrons and the atomic limit of localised electrons – the situation becomes much more complicated. The physics is determined by the competition between kinetic energy and Coulomb interaction, and the general N-particle state is not just a Slater determinant of one-particle states. The Hamiltonian is diagonal neither in real nor in Fourier space. This observation is the starting point for attempting a many-body modelling that describes precisely these counteracting tendencies.

The simplest model that contains the interplay of delocalisation due to the kinetic energy gain and the localisation due to Coulomb interactions is due to John Hubbard, Martin Gutzwiller and Junjiro Kanamori [18–22]:

$$H = \sum_{ij\sigma} t_{ij} c^{\dagger}_{i\sigma} c_{j\sigma} + \sum_i U n_{i\uparrow} n_{i\downarrow} \tag{9}$$

It describes the competition between the energy gain due to delocalisation of the electrons and the Coulomb interaction. Indeed, the expectation value of the double occupation $\langle n_{i\uparrow} n_{i\downarrow} \rangle$ is finite in the delocalised state, leading to an interaction energy that can – for narrow band systems – outweigh the kinetic energy contribution.

The microscopic justification of this Hubbard model relies on the introduction of a localised basis set, spanning the low-energy Hilbert space of the one-particle part of the Hamiltonian, and on the calculation of the effective Coulomb interaction acting on those degrees of freedom. To simplify the discussion, let us assume for the moment that we are dealing with a system where the low energy band states can be derived from a single atomic orbital that is replicated to all atomic sites R. This atomic orbital $\chi_R(r)$ is then a Wannier function of the system, and in this case, the Fourier transform of the Bloch eigenstate $\chi_k(r)$. When writing the full crystal Hamiltonian in the basis of the atomic orbitals, among the matrix elements of the Coulomb interaction,

$$U(R, R') = \int \mathrm{d}r \mathrm{d}r' |\chi_R(r)|^2 |\chi_{R'}(r)|^2 v_{\text{screened}}(r, r') \tag{10}$$

the onsite ($R = R'$) term that describes the Coulomb energy cost of creating doubly occupied atomic sites dominates for obvious reasons.[9]

[9] The interaction $v_{\text{screened}}(r,r')$ is not simply the bare Coulomb interaction $1/(|r - r'|)$ but rather a partially screened version of it. This issue will be the subject of Sect. 12, which describes recent developments in the field.

For an account of the microscopic motivation and further discussion of the physics, we refer the reader to the original papers [18–22]. In one dimension, the model (9) is exactly solvable and exhibits the effects special to this case, in particular Tomonaga–Luttinger behaviour and spin-charge separation. Here, we focus on the basic physical effects that this model displays in higher dimensions. Indeed, apart from the one-dimensional case this model allows for yet another limit where the exact solution can be investigated, which is the case of infinite connectivity of the lattice [23].

The phase diagram for this case has been explored in detail in the literature (see, e.g. [5]). At sufficiently low temperatures it displays a metal–insulator transition as a function of the interaction, as expected from the qualitative discussion of the atomic and band limits above. The transition – except at zero temperature – is of first order, displaying a pronounced coexistence region, where both an insulating and a metallic phase can be stabilised. The spinodals end in a high-temperature critical point, above which crossovers between bad metal and semiconducting behaviours are found. While formally the exact solution is in infinite dimensions (that is for a lattice model where each site has an infinite number of nearest neighbours), the above scenario is believed to be a reasonable approximation in three dimensions in regimes not too close to the metal–insulator transition. It is therefore more than an academic exercise to describe how the above solution can be obtained. This is the subject of the following section, devoted to dynamical mean field theory (DMFT).

6 Dynamical Mean Field Theory

The basic idea of DMFT is to replace a lattice problem (or in the case of a solid, the correlated orbitals of an atom/a cluster of atoms, defined within a localised basis set) by an effective local system, coupled to a bath and subject to a self-consistency condition, in analogy to conventional Weiss mean field theory in statistical mechanics. In contrast to the latter, however, the intervening mean field is energy-dependent, hence the notion of a *dynamical* MFT.[10]

Let us illustrate the method on the example of the single-band Hubbard model, as defined by the Hamiltonian above, which we rewrite in the more general form

$$H = \sum_{ij\sigma} t_{ij} \left(c^{\dagger}_{i\sigma} c_{j\sigma} + c^{\dagger}_{j\sigma} c_{i\sigma} \right) + H_{\text{int}} \tag{11}$$

indicating that the many-body term H_{int} could contain more general local interactions. Dynamical mean field theory associates with this Hamiltonian an auxiliary *local* problem, tailored such as to reproduce the physics of a single site within the

[10] DMFT has been the subject of several extended review articles, see, e.g. [24–26].

lattice problem. To this effect, the site of the auxiliary local problem is coupled to a *bath*, which is determined such as to mimic the effect of the other lattice sites on the one that is treated explicitly. Even before the advent of dynamical mean field theory, the problem of a single site coupled to a bath had received much attention: this is the celebrated Anderson impurity problem describing the physics of impurities in metallic host systems. The only difference when using the Anderson impurity problem as an auxiliary system within dynamical mean field theory is the requirement that the bath has to be determined self-consistently instead of simply being given by the host density of states.

Mathematically, the auxiliary problem is defined by the "Anderson impurity" Hamiltonian

$$H = \sum_l \left(\varepsilon_l d_{l\sigma}^\dagger d_{l\sigma} + V_l c_{0\sigma}^\dagger d_{l\sigma} + V_l^* d_{l\sigma}^\dagger c_{0\sigma} \right) + H_{\text{int}}, \tag{12}$$

or, equivalently, by the action

$$\begin{aligned} S = &- \int\int \mathrm{d}\tau \mathrm{d}\tau' \sum_\sigma c^\dagger(\tau') \left(\delta(\tau - \tau') \partial_\tau - \Delta(\tau - \tau') \right) c(\tau) \\ &+ \int \mathrm{d}\tau H_{\text{int}} \end{aligned} \tag{13}$$

where the hybridisation function of the impurity

$$\Delta(\omega) = \sum_l \frac{|V_l|^2}{\omega - \varepsilon_l} \tag{14}$$

is parameterised by the bath hybridisations V_l and energies ε_l.

This Hamiltonian or action describes the physics of one of the original lattice sites (labelled here as 0) coupled to a bath (operators d, $d^\dagger$) through a hybridisation V_l. The bath has an infinite number of degrees of freedom (labelled by l) of energies ε_l. Within dynamical mean field theory, the Anderson impurity model is reinterpreted in the following way: the impurity site 0 represents an arbitrary site of the original lattice, and the bath plays the role of the mean field representation of the rest of the lattice. In contrast to the original ideas of Anderson, who wrote an impurity model in order to describe a physical impurity in a (given) host material, the impurity within the DMFT context is representative of a correlated orbital at a given site of a translationally invariant solid. The bath is thus a quantity that has to be determined self-consistently in order to restore the translational invariance of the lattice.

In practise, the computational task consists of calculating the local Green's function

$$G^{\mathrm{imp}}_{LL'\sigma} = -\left\langle \hat{T}\, c_{L\sigma} c^{\dagger}_{L'\sigma} \right\rangle \tag{15}$$

of the above local impurity model. Here, the brackets denote the thermodynamical average taken with the density matrix of the Anderson impurity model Hamiltonian (12), and $\hat{T}$ is the time-ordering operator. For the explicit calculation of the Green's function a variety of techniques ranging from Monte Carlo simulations [27] to approximate schemes are available. The self-consistency condition then imposes that all equivalent sites behave in this same way. This requirement eventually determines the parameters of the Anderson impurity model. Mathematically speaking, one imposes the local Green's function G of the solid to equal the impurity Green's function G^{imp}. To this effect, the self-energy of the impurity model

$$\Sigma_{\mathrm{imp}} = \mathcal{G}_0^{-1} - G^{-1} \tag{16}$$

is calculated and used as an approximation to the full self-energy of the lattice. The *bare propagator of the impurity model*, $\mathcal{G}$, also called the "Weiss dynamical mean field", is related to the impurity hybridisation function via

$$\mathcal{G}_0^{-1} = \omega - \Delta(\omega). \tag{17}$$

Finally,

$$G(\imath\omega_n) = \sum_{\mathbf{k}} \left[\imath\omega_n + \mu - H_0(\mathbf{k}) - \Sigma^{\mathrm{imp}}(\imath\omega_n)\right]^{-1}. \tag{18}$$

In practise, the set of equations (15)–(18) is solved iteratively in a cycle starting from a guess for the bath parameters ε_1 and V_1, solving the impurity model, inserting the corresponding self-energy into the self-consistency (18), recalculating the bath from Dyson's equation and using the result to update the impurity model.

At convergence, an estimate for the local part of the physical Green's function G is obtained. From G, the spectral function

$$A(\omega) = -\frac{1}{\pi} \Im Tr G(\omega), \tag{19}$$

where the trace is over orbital degrees of freedom, is obtained. DMFT thus gives naturally access to the local spectral function, containing many-body effects beyond simple one-particle densities of states, and allowing for quite direct comparison to photoemission spectroscopy, even as a function of temperature.[11]

[11] Calculating photoemission intensities strictly speaking involves further modelling steps, including in particular matrix elements describing the coupling of the light field to the electrons of the solid. We do not enter into this discussion here, but restrict ourselves to discussing the spectral function.

Assuming the impurity self-energy to be a reasonable approximation to the full self-energy of the solid, momentum-resolved spectral functions can also be calculated:

$$A(k,\omega) = -\frac{1}{\pi}\Im TrG(k,\omega) \tag{20}$$

where the momentum-resolved Green's function is given by

$$G(k,\omega) = \left[\omega + \mu - H_0(\mathbf{k}) - \Sigma^{\mathrm{imp}}(\omega)\right]^{-1}. \tag{21}$$

In practice, the self-consistency loop is most often performed within the finite temperature Matsubara formalism, giving access to Green's functions on the imaginary time or frequency axis, and an analytical continuation has to be performed, e.g. using a maximum entropy algorithm.

7 Electronic Structure Calculations for Correlated Materials

Until the late 1990s, work in theoretical modelling of materials properties could quite generally be attributed to one of two general classes: "first-principles calculations" or "model approaches". The former class is appealing in that it treats the solid ab initio (that is, without any adjustable parameters). The electronic Coulomb interactions, however, are dealt with within static mean field theory. We have explained above why this strategy will fail in the description of spectral properties of solids with localised electrons. The latter strategy, explained above by the example of the Hubbard model, consists of studying the interplay of localised and delocalised behaviour within the simplest models that incorporate the competition between kinetic energy and Coulomb interactions. While very successful in assessing the basic mechanisms, e.g. of correlation-driven metal–insulator transitions, this approach obviously takes a very simplistic view on the chemistry of a compound, namely by including only one band and an effective hopping between sites. It has no say on the effect of multi-orbital Coulomb correlations, hybridisation between different bands, the influence of crystal field splittings, etc.

To address a given compound, an attractive way to arrive at a materials-specific description is to calculate hoppings, hybridisations and crystal fields within band structure techniques, and then to use the resulting one-particle Hamiltonian as a starting point for a *multi-orbital* Hubbard-type Hamiltonian that can be treated within many-body techniques. This strategy is realised in the combination of density functional theory with dynamical mean field theory, the so-called "LDA + DMFT" scheme, which was first proposed and implemented in independent work

by Lichtenstein and Katsnelson [28] and a research collaboration between the group of V. Anisimov and G. Kotliar [29].

The basic idea of constructing a local model for the purpose of calculating a local self-energy as an approximation to the full many-body self-energy of the system carries over directly from the model context to the case of a real solid. The most basic version of the combined "LDA + DMFT" scheme can be viewed as a DMFT solution of a multi-orbital Hubbard model with parameters calculated from DFT − LDA. The impurity represents the correlated orbitals in the solid, and the self-consistency condition attributes the same self-energy to all equivalent correlated atoms up to rotations in orbital space.

Besides varying techniques for solving the impurity problem, modern implementations mainly differ in issues related to the orbitals used for defining the interaction terms and the notion of locality in the DMFT context [30], the basis set of the LDA implementation and the self-consistency condition [31], as well as the possibility of an update of the one-particle Hamiltonian [32, 33]. LDA + DMFT was even implemented within the multiple-scattering formalism of the Korringa–Kohn–Rostocker method [34].

8 Applications of the Combined LDA + DMFT Scheme

The very first DMFT calculations based on DFT band structure input were performed by Anisimov et al. [29] for doped $LaTiO_3$ and by Lichtenstein and Katsnelson [28] for NiO and $TmSe_2$. In the following years, LDA + DMFT was successfully applied to a number of materials, ranging from transition metals [35–37], their oxides [38–56] and sulphides [57, 58], to actinide or rare earth systems [33, 59–62], and more recently to iron pnictide compounds [63–70], organic materials [71] and thermoelectrics [12, 72, 73]. DMFT-inspired techniques have been applied to argue in favour of the importance of strong many-body effects for ligand binding in haemoglobin [74] and make their way into the exploration of oxide heterostructures [75–77]. In total, several hundred pieces of work have been carried out using combined density functional dynamical mean field techniques so far. A review up to 2006 is given in [78]. More specialised review articles focussing on specific aspects can be found in [26, 79–83]. We will not enter into an exhaustive discussion of the numerous applications of DMFT, but present a choice – guided by the subjective tastes of the author – of three different materials classes: transition metals, transition metal oxides and rare earth pigments.

8.1 Transition Metals: The Example of Elemental Manganese

Transition metals account for some of the very early applications of the combined LDA + DMFT scheme, with studies on iron and nickel [28] and on elemental manganese [35, 36], which immediately followed the initial proposals of the method. Later on, extensive studies involving detailed comparisons with angle-resolved photoemission have been presented for all the late transition metals [84–89].

Transition metals of the 3d series mostly realise simple bcc, fcc or simple hexagonal structures. An exception is manganese: the stable phase under normal conditions is the so-called α-Mn phase, a complex derivative of the bcc structure with 58 atoms per unit cell [90]. Nevertheless, it is possible to explore practically the full phase diagram at room temperature by growing Mn on appropriate substrates. On a Cu_3Au substrate, an fcc (or, more precisely, fct) structure[12] is realised, corresponding to the so-called γ-Mn. Early on, [35] presented a joint angle-resolved photoemission and LDA + DMFT study of this phase. The starting point was the puzzling observation of entirely undispersive features at about -2.5 to -2.7 eV binding energy in the ARPES spectra (feature B in Fig. 1), coexisting with quasi-particle bands (feature A in Fig. 1) around the Fermi level. These came as a surprise because simple transition metals were, until then generally considered as weakly correlated systems, i.e. possibly displaying some quasi-particle lifetime effects but otherwise well-described by band theory. The comparison with computed k-resolved spectral functions from combined LDA + DMFT indeed allowed identification of the observed undispersive and broad peak in the ARPES spectra with a *Hubbard band*, a many-body satellite feature corresponding to electron removal processes from localised 3d states. At the same time, this was one of the early proofs of LDA + DMFT indeed being able to describe quasiparticle renormalisations and atomic-like Hubbard features on an equal footing for realistic materials. It was argued that manganese – despite similar values of the Hubbard interactions U – is more prone to electronic correlations than other transition metals: this is due to the half-filled 3d shell, which, in the presence of the relatively strong Hund's coupling $J \sim 0.9$ eV that characterises the elemental 3d systems, favours strong correlations due to the limited number of available screening channels. This effect has recently attracted much attention in oxides (see, e.g. [91] and references therein) and iron pnictides [92]. The early LDA + DMFT study [35] for elemental manganese has been continued in systematic follow-up investigations not only on spectral properties but also on the energetics [93], giving access to structural properties and the bulk modulus.

Furthermore, this system has served as a test ground for comparisons between LDA + DMFT using a numerically exact Monte Carlo scheme for the solution of the DMFT equations and simplified schemes based on the "Disordered Local Moment" (DLM) approach and perturbative solver schemes (in particular the spin-polarized T-matrix fluctuation-exchange (SPTF) approximation) [94]. It was

[12] We note that, crystallographically, a tetragonally distorted fcc phase, is described as a bct lattice.

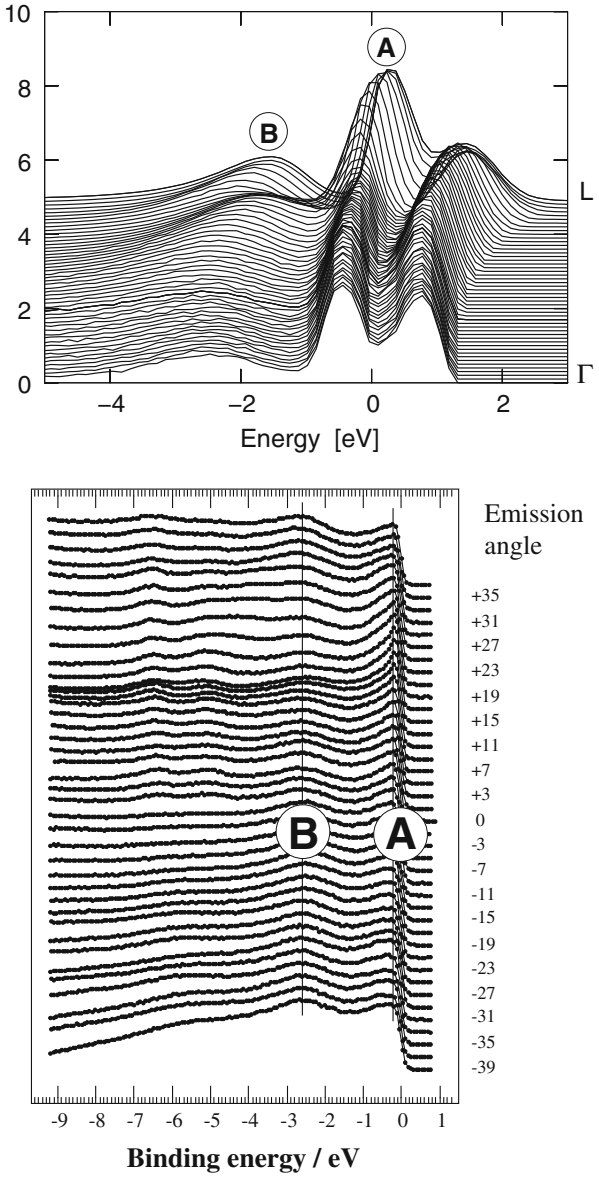

Fig. 1 Momentum-resolved spectral functions $A(\mathbf{k},\omega)$ of elemental manganese in its paramagnetic γ-phase, in comparison to experimental ARPES spectra for different emission angles, corresponding approximately to the path in k-space between Γ to L. A dispersive quasi-particle band (feature A) is visible close to the Fermi level (chosen to be the origin of the energy scale). A second, less dispersive feature (peak B) appears at -2 to -3 eV binding energy, and is identified as a lower Hubbard band. Adapted from [35]

found that, while a combination of DLM and SPTF is indeed successful in the weak correlation regime, or, more generally, in capturing quasi-particle renormalisations in a similar way to LDA + DMFT, it is unsuitable for the description of higher-energy features such as Hubbard bands in the more strongly correlated regime.

8.2 Transition Metal Oxides: The Examples of $YTiO_3$ and Sr_2IrO_4

Transition metal oxides provide classical examples of correlated behaviour, ranging from weakly correlated Fermi liquids to strong coupling Mott insulators. The whole range of behaviours is, e.g. realised in the series of d^1 perovskite compounds $SrVO_3$, $CaVO_3$, $LaTiO_3$ and $YTiO_3$. These compounds, while isoelectronic and (nearly) isostructural, display radically different behaviours: the vanadates are moderately correlated metals with a mass enhancement factor of about 2, while the titanates are insulating. LDA + DMFT calculations for these compounds were able to unravel the underlying mechanism: tiny differences in the orbital occupations that are induced by $GdFeO_3$-type distortions at the band structure level are amplified by the electronic Coulomb interactions such as to lead to nearly complete orbital polarisation. For $YTiO_3$, for example, the orbital polarisation results in an effective single-band model; this reduction of the degeneracy suppresses the kinetic energy, and even moderate Coulomb interactions fully localise the system. Indeed, as is well known from studies of multi-orbital Hubbard models, the critical interaction for the formation of the insulating state is lowest for the one-band case, and increases with degeneracy (see, e.g. [95]).

A similar effect, albeit through an entirely different mechanism, is realised in the 5*d* iridate Sr_3IrO_4. The number of works on iridates has exploded recently due to a doubly renewed interest in these materials: on the one hand, strong spin-orbit interactions in these compounds make them ideal candidates for studying non-trivial topological effects concerning surface states. On the other hand, and independently of the questions of topological behaviour, 5*d* compounds have come into focus for studying correlations. Indeed, in strong contrast to the naive expectation of weak correlation effects due to the quite extended nature of 5*d* states, several iridium oxides have been found to display insulating phases that cannot be rationalised within a band picture. This is the case for Sr_3IrO_4, which exhibits insulating behaviour at all temperatures although each Ir site accommodates five electrons. Sr_2IrO_4 has a tetragonal crystal structure whose symmetry is lowered from the K_2NiF_4-type, also found in Sr_2RuO_4 and La_2CuO_4, by an 11°˜ rotation of its IrO_6 octahedra around the *c*-axis. Below 240 K, canted-antiferromagnetic (AF) order sets in [96], and this phase has triggered much experimental and theoretical work recently [97–101], highlighting in particular the importance of the spin-orbit coupling. While LDA + U is able to open the gap in the low-T phase thanks to the magnetic structure, the paramagnetic phase has so far been accessible only in LDA + DMFT calculations.

In [102], the very first LDA + DMFT calculations for iridates were performed, and it was shown that the combined effect of spin-orbit coupling and structural distortions is strong enough to suppress the effective degeneracy of the coupled spin-orbital degrees of freedom such that even moderate Coulomb interactions induce a Mott localised state. The large spin-orbit coupling of about 0.4 eV splits the t_{2g}-states into a quartet of states, commonly labelled $j_{\mathrm{eff}} = 3/2$, and a higher lying doublet $j_{\mathrm{eff}} = 1/2$. Each state is doubly degenerate in $\pm m_j$. In LDA, the four

$j_{\mathrm{eff}} = 3/2$ states are almost filled, and thus the $j_{\mathrm{eff}} = 1/2$ states only slightly exceed half-filling. The spin-orbital polarisation is enhanced when Coulomb correlations are taken into account: within LDA + DMFT, the Wannier orbital $j_{\mathrm{eff}} = 1/2$ is exactly half filled, and the upper Hubbard band is of $j_{\mathrm{eff}} = 1/2$ type only. This solution of the LDA + DMFT equations corresponds to an insulator with a Mott gap of the size of the optical gap measured at room temperature (about 0.26 eV [103]). We are thus dealing with a state exhibiting a "spin-orbital order" in the sense of a well-defined j_{eff} quantum number. As shown explicitly in [102], in Sr_2IrO_4 the Hubbard interactions are large enough to induce a Mott insulating state in a half-filled one-orbital but not in a quarter-filled two-orbital or a one-sixth-filled three-orbital system. The reduced effective spin-orbital degeneracy is thus the reason for the insulating nature of Sr_2IrO_4. This effect is analogous to the suppression of *orbital* degeneracy, albeit purely induced by crystal field splittings, discussed above for $YTiO_3$ [49]. In Sr_2IrO_4, the suppression of *spin-orbital* fluctuations is a consequence of the combined effect of Coulomb correlations, spin-orbit coupling and tetragonal distortions.

8.3 Rare Earth Pigments

In rare earth oxides, sulphides or fluorosulphides Coulomb interactions are strong enough to localise entirely the rare-earth 4*f*-electrons. These states do not form bands but rather atomic multiplets. In this case, an excellent approximation to the many-body self-energy is provided by the purely atomic one. This is the content of the so-called Hubbard-I approximation, which has been shown to be extremely successful in Mott-insulating *f*-electron compounds [32, 104, 105].

Figure 2 displays the spectral function of CeSF, a fluorosulphide used as a red pigment. The states corresponding to the *f*-states are clearly distinguished as dispersionless atomic levels. Interestingly, however, the gap does not open between *f*-states, nor between Ce-*d* and *f* states, but is rather of interatomic character: *p*–*f*. This is a highly unusual situation and has implications for the optical properties of the compound. Very recently, in [105], first-principles calculations were pushed beyond LDA + DMFT in order to calculate optical absorption properties and – using an intermediate length scale modelling technique due to Kubelka and Munk – even the *colour* of the compound. This example demonstrates how LDA + DMFT techniques can be taken further towards predictive calculations for functional materials coming closer to the ultimate goal of computational materials design, even for materials where the failure of band theory is a qualitative one.

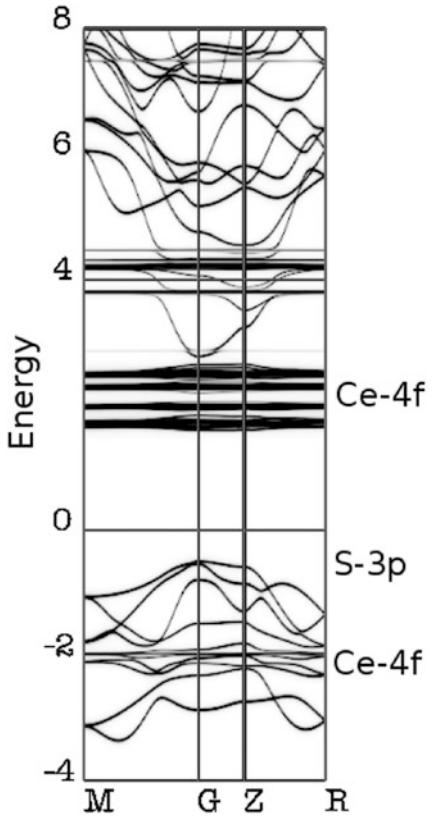

Fig. 2 Momentum-resolved spectral functions $A(\mathbf{k},\omega)$ of CeSF. The gap opens between the S-3*p* states and the upper Hubbard band (split into crystal field levels) of the Ce-4*f* states. Note that CeSF is an f^1-compound without magnetic order, and would not be insulating in any single-particle picture. Adapted from [105]

9 Beyond "Solving Models": LDA + DMFT in the Basis of Bloch Waves

Historically, the first LDA + DMFT calculations consisted of the extraction of the parameters of a many-body Hamiltonian from first-principles calculations and then solving the problem by DMFT. It was soon realised, however, that there is no need to perform the LDA part of the calculation on the basis of localised orbitals used to define the impurity problem.

Indeed, it is possible to distinguish between the complete basis set of the problem, in which the Green's function of the solid will be formulated, and a suitably chosen set of localised Wannier-like functions $|w^{\alpha,\sigma}_{\mathbf{k}m}\rangle$. The latter functions span the "correlated" subspace $\mathcal{C}$ of the full Hilbert space, in which the local problem will be formulated and corrections beyond LDA due to many-body correlations will be considered. The index m is an orbital index within the correlated subset, α denotes the atom in the unit cell and σ the spin degree of freedom. Different choices for the construction of the localised orbitals are possible. Our

discussion follows those in [30, 64], where two different options were explored respectively: maximally-localised Wannier functions [30] and atomic orbitals that are then promoted to Wannier-like functions by an orthonormalisation procedure [64].

In these schemes, projections of quantities of interest on the subset $\mathcal{C}$ are obtained using the projection operator

$$\hat{P}^{\alpha,\sigma}(\mathbf{k}) = \sum_{m \in \mathcal{C}} \left| w_{\mathbf{k}m}^{\alpha,\sigma} \right\rangle \left\langle w_{\mathbf{k}m}^{\alpha,\sigma} \right|. \tag{22}$$

The effective impurity model is constructed for the correlated subset $\mathcal{C}$. It is defined by a bath Green's function $\mathcal{G}_{mm'}^{0,\sigma}(i\omega_n)$ and Hubbard–Kanamori interaction parameters $U_{mm'm''m''}$. By solving this model (e.g. by numerically exact Monte Carlo simulations) one obtains the impurity Green's function $G_{mm'}^{\sigma,\mathrm{imp}}(i\omega_n)$ as well as the impurity self-energy

$$\Sigma_{mm'}^{\sigma,\mathrm{imp}}(i\omega_n) = \left(\mathcal{G}_{mm'}^{\sigma,0}(i\omega_n)\right)^{-1} - \left(G_{mm'}^{\sigma,\mathrm{imp}}(i\omega_n)\right)^{-1}. \tag{23}$$

For the formulation of the self-consistency condition relating the lattice Green's function of the solid to the impurity model, it is convenient to choose the Bloch basis $|\psi_{\mathbf{k}\nu}^{\sigma}\rangle$ as the complete basis set of the problem, since it is a natural output of any electronic structure calculation. The Green's function of the solid expressed in this basis set is given by

$$G_{\nu\nu'}^{\sigma}(\mathbf{k}, i\omega_n) = \left[\left(i\omega_n + \mu - \varepsilon_{\mathbf{k}\nu}^{\sigma}\right)\delta_{\nu\nu'} - \Sigma_{\nu\nu'}^{\sigma}(\mathbf{k}, i\omega_n) \right]^{-1}, \tag{24}$$

where $\varepsilon_{\mathbf{k}\nu}^{\sigma}$ are the Kohn–Sham eigenvalues and $\Sigma_{\nu\nu'}^{\sigma}(\mathbf{k}, i\omega_n)$ is the approximation to the self-energy obtained by "upfolding" the impurity self-energy:

$$\Sigma_{\nu\nu'}^{\sigma}(\mathbf{k}, i\omega_n) = \sum_{\alpha,\, mm'} P_{\nu m}^{\alpha,\sigma *}(\mathbf{k}) \Delta\Sigma_{mm'}^{\sigma,\mathrm{imp}}(i\omega_n) P_{m'\nu'}^{\alpha,\sigma}(\mathbf{k}), \tag{25}$$

where $P_{m\nu}^{\alpha,\sigma}(\mathbf{k}) = \langle w_{\mathbf{k}m}^{\alpha,\sigma} | \psi_{\mathbf{k},\nu}^{\sigma} \rangle$ are the matrix elements of the projection operator, (22) and

$$\Delta\Sigma_{mm'}^{\sigma,\mathrm{imp}}(i\omega_n) = \Sigma_{mm'}^{\sigma,\mathrm{imp}}(i\omega_n) - \Sigma_{mm'}^{dc}. \tag{26}$$

Here, $\Sigma_{mm'}^{\sigma,\mathrm{imp}}$ is the impurity self-energy, (23), expressed in the local orbitals, and $\Sigma_{mm'}^{\mathrm{dc}}$ is a double-counting correction, which is meant to remove Coulomb correlations on the correlated states already contained in the LDA. As in LDA + U, the double counting correction is one of the weaknesses of the scheme: it is not possible

to derive microscopically the double counting correction, so that different physically motivated schemes are used; see [106] for a systematic comparison and discussion.

The local Green's function is obtained by projecting the lattice Green's function to the set of correlated orbitals m of the correlated atom α and summing over the full Brillouin zone:

$$G^{\sigma,\mathrm{loc}}_{mm'}(i\omega_n) = \sum_{\mathbf{k},\nu\nu'} P^{\alpha,\sigma}_{m\nu}(\mathbf{k}) G^{\sigma}_{\nu\nu'}(\mathbf{k}, i\omega_n) P^{\alpha,\sigma *}_{\nu' m'}(\mathbf{k}). \tag{27}$$

In principle, the local quantities $G^{\sigma,\mathrm{loc}}_{mm'}(i\omega_n)$ and $\Delta\Sigma^{\sigma,\mathrm{imp}}_{mm'}(i\omega_n)$ also carry an index α, which we suppress for better readability.

The self-consistency condition of DMFT relates the *local* Green's function, (30), to that of the effective impurity problem:

$$\mathbf{G}^{\sigma,\mathrm{loc}}(i\omega_n) = \mathbf{G}^{\sigma,\mathrm{imp}}(i\omega_n). \tag{28}$$

The projectors are in general non-square matrices. They reduce to square matrices only in the case when the number of Kohn–Sham bands contained in the chosen window at every k-point equals the number of correlated local orbitals to be constructed.

Finally, we mention that it is not only the possibility to relate more realistically the *parameters* of a Hubbard-like model to the microscopic electronic structure that has enabled progress towards materials-specific predictive calculations. A further advance concerns the possibility of updating the Hamiltonian itself once an improved estimate for the Green's function and therefore the charge density has been calculated. This second self-consistency loop is represented as outer loop in the flow chart of Fig. 3.

The charge-density correction $\Delta\rho$ may be expressed as

$$\begin{aligned} \Delta\rho(r) &= \left\langle r \middle| \hat{G} - \hat{G}_{\mathrm{KS}} \middle| r \right\rangle \\ &= \left\langle r \middle| \hat{G}_{\mathrm{KS}} \Delta\hat{\Sigma} \hat{G} \middle| r \right\rangle. \end{aligned} \tag{29}$$

and the updated Hamiltonian is constructed using the Kohn–Sham potential corresponding to this new density.

An interesting comment is in order here: obviously, the correction would vanish if the exact density functional was used. The charge update is therefore a correction that is to be viewed on a different level to the above discussed failures of the band picture for spectroscopic properties: it is necessary for systems where the LDA is a poor approximation to the density functional which can be corrected by DMFT. In practice, it has been shown to be important, for example, for systems with localised *f*-electrons [32, 33].

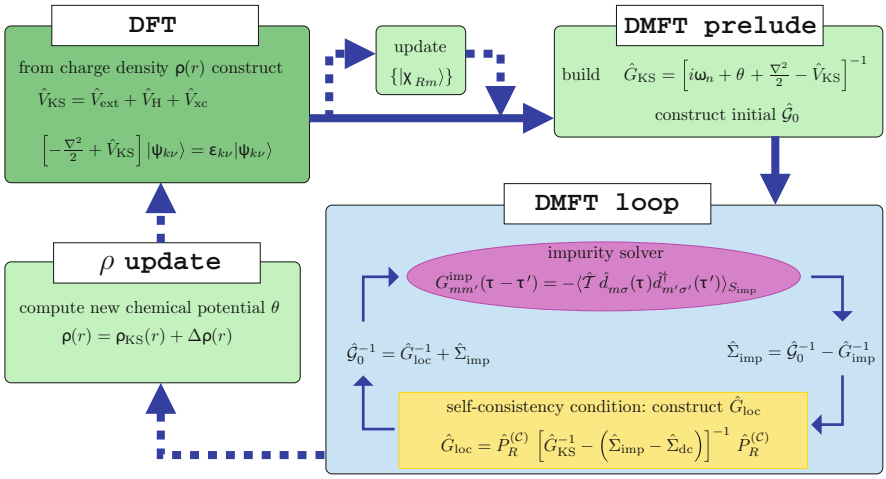

Fig. 3 Self-consistency loop for LDA + DMFT. The charge density ρ determines the Kohn–Sham (KS) potential $V_{\rm KS}$, from which KS eigenvalues $\varepsilon_{k\nu}$ and eigenfunctions $\psi_{k\nu}$ are calculated. The KS Green's function is constructed and passed on to the DMFT cycle. The DMFT loop consists of (1) solving the effective impurity problem for the impurity Green's function, hence obtaining an impurity self-energy, (2) combining the self-energy correction with the KS Green's function in order to obtain the local Green's function $G_{\rm loc}$ projected in the correlated subset and (3) obtaining an updated Weiss mean-field. An initial guess for the Weiss dynamical mean-field must be made at the beginning of the DMFT loop, e.g. by choosing $\hat{\mathcal{G}}_0^{\rm init} = \hat{P}^{(\mathcal{C})}\hat{G}_{\rm KS}\hat{P}^{(\mathcal{C})}$. Once the DMFT loop is converged, the chemical potential is updated in order to ensure the correct electron number, and the new charge density (including many-body effects) is constructed. This new density determines a new KS potential. In principles, it is also possible to update in addition the set $\{|\chi_m\rangle\}$ when preparing for the next DMFT loop. The process is iterated until the charge density, the impurity self-energy and the chemical potential are converged. Adapted from [30]

From the computational point of view, the solution of the impurity problem remains quite generally the numerically costly step, the update of the Hamiltonian being at the cost of a DFT calculation without self-consistency.

Further details on modern LDA + DMFT implementations and applications to electronic structure calculations can be found, e.g., in [30, 64].

10 Cluster Extensions of LDA + DMFT

When used within electronic structure calculations, the dynamical mean field approximation consists of assuming that the local Green's function can be well represented by a purely local self-energy, and that this self-energy can be obtained within the DMFT self-consistency cycle. Cluster extensions of DMFT [107] relax this assumption and allow for an explicitly k-dependent many-body self-energy. While computationally expensive, using cluster-DMFT schemes within realistic electronic structure calculations is straightforward and has been pioneered in

several cases [108–110]. Interestingly, while the application of cluster DMFT schemes to the two-dimensional Hubbard model is not unambiguous, since a choice for the embedding of the cluster into the lattice has to be made, in realistic compounds specific choices for the cluster are often imposed by nature.[13] This is the case, for example, for vanadium dioxide, which undergoes a structural transition to a dimerised phase at low temperatures. Using a vanadium dimer as impurity site in LDA + DMFT calculations is thus a natural choice, and such calculations have indeed been able to assess quantitatively the physics of the celebrated metal–insulator transition in VO_2. The calculations of spectral properties in [108, 115–118] have been followed by extensions addressing the optical properties of this compound [9, 10, 119].

We do not enter here into the decade-long discussion about the relative importance of structural distortions (Peierls mechanism) and electronic correlations (Mott mechanism) for the metal–insulator transition (see, e.g. the references in [119]). Nevertheless, we mention the following interesting observation [117, 118] resulting from an analysis of the cluster-DMFT results: for the purpose of calculating the momentum-resolved spectral function, the many-body self-energy can be replaced by an orbital-dependent[14] yet *static* potential, which results in shifting apart bonding and antibonding a_{1g}-states and in this way opening the insulating gap. The spectral function of the insulating phase is thus well-described by a single-particle picture,[15] and it is therefore no surprise that any one-body theory that in some way applies a scissor operator shifting apart bonding and antibonding states compared to the DFT-LDA picture succeeds in opening the gap. This is in contrast to other vanadium oxides such as V_2O_3 where the dynamics of the self-energy is necessary to describe the insulating character of the paramagnetic phase.

Interestingly, however, the physics of the *metallic* phase of vanadium dioxide is much harder to describe theoretically: indeed, in this phase, substantial lifetime effects broaden the features in the spectral function, transport is of "bad-metal"-type and the susceptibility displays pronounced local moment behaviour. As this has been analysed in detail [117, 118], it is thus fair to say that vanadium dioxide is one of the probably rare compounds where correlation effects are much stronger in the metallic than in the insulating phase.

11 Relation to Other Electronic Structure Methods

At this stage, we return to the relatively fundamental considerations of Sect. 3. There, correlations were mathematically defined as a non-vanishing correlator $C_{AB} := \langle AB \rangle - \langle A \rangle \langle B \rangle$, and it was pointed out that any single-particle picture

[13] The same is true for quasi-one-dimensional systems, where one-dimensional chains provide natural entities to be treated as clusters; see the applications of "chain-DMFT" in [111–114].

[14] Thus non-local in the electronic structure sense.

[15] Even though the latter is *not* derived from a local potential.

is unable to produce a non-vanishing value for this quantity. Focussing on spectroscopic properties in the following, we therefore make a fundamental distinction between theories that have the potential to include correlation effects in the form of a finite $C_{n_R n_R}$[16] and theories that can eventually be cast into a band picture.

Within this definition, it is interesting to note that the widely used LDA + U scheme, a static mean field approximation to a multi-orbital Hubbard-like Hamiltonian, falls strictly speaking into the latter category. Indeed, the success of LDA + U for "correlated materials" is quite generally based on the fact that it is usually used for broken-symmetry phases, where vanishing values of the double-occupancy of an orbital can be captured without having non-trivial values of $C_{n_R n_R}$ (see the discussion of magnetic phases above). In most classical examples, the opening of a gap within LDA + U can be understood as a relative shift of spin-up and spin-down states with respect to each other, without the necessity of going beyond the single-particle picture.[17] An interesting question is then that of the role of fluctuations beyond LDA + U for spectral properties: does LDA + DMFT reduce to LDA + U in this case? Remarkably, [120] advocates that, on a quantitative level, the answer is negative: both, the size of the gap and the width of the Hubbard bands are modified by the dynamical effects.

We stress that in some cases it is necessary to specify how a theory is used in practice. The GW method, for example, is a (potentially finite-temperature-) many-body approximation to the many-body self-energy that can be fully dynamic (that is, energy-dependent) and in general includes real and imaginary parts. Due to its perturbative nature, it may not be suitable to describe materials in their strong coupling regime, but still, correlation effects (e.g. quasi-particle lifetimes) are included beyond the one-particle description. However, in practice, the GW approximation is often used as a zero-temperature scheme to generate static corrections to a Kohn–Sham band structure, lifetime effects are neglected and densities of quasiparticle states replace the true spectral function. Recently, several pieces of work have pioneered the GW scheme for the magnetic phases of transition metal oxides or *f*-electron compounds [121–124]. These advances are particularly interesting since – in contrast to LDA + U – the gap opening is obtained without any ambiguities related to the choice of Hubbard interactions or double counting; the underlying mechanism is, however, the same as in LDA + U, and the final picture is based on an effective band theory, without the need for generating non-trivial values of C. To our knowledge, a systematic analysis of how the GW approximation, used as a true many-body scheme, would perform concerning the quantitative questions concerning the width of the Hubbard bands and gap size compared to LDA + U has not yet been carried out.

[16] With $n_R = \Sigma_{L,\sigma} n_{RL\sigma}$ the number operator of electrons in localised orbitals L on atom R with spin σ.

[17] The situation is somewhat more subtle when more exotic kinds of ordering are involved, such as orbital- or charge order. Still, the general remark about the resulting spectrum being strictly a band structure holds.

It is clear on general grounds, that – within the perspective of addressing correlated materials from first principles – the most attractive feature of the GW approximation is its first-principles treatment of the long-range Coulomb interaction, including not only long-range exchange contributions but also dynamical screening effects. This is the motivation for the recent quest for improved first-principles many-body schemes at the interface of many-body perturbation theory and dynamical mean field techniques. We will come back to this point below.

12 Making LDA + DMFT Parameter-Free: Strategies for Calculating Hubbard Interactions

The dream of scientists working on electronic structure calculations is twofold: first, to *understand and describe* properties of condensed matter within a parameter-free modelling, and second – and this is an even more ambitious goal – to *predict* properties of yet unknown materials. DMFT-based electronic structure techniques have met with tremendous success concerning the first issue, and, currently, strong efforts are being made to work towards the second.

An important bottleneck in this enterprise is to make the theory indeed fully parameter free. Most of the early LDA + DMFT work considered Hubbard interactions as adjustable parameters, fitted to experiments or transferred from "similar compounds". None of these strategies is compatible with fully ab initio predictive electronic structure calculations. For this reason, a whole line of research has developed over the last decade to explore techniques to calculate the effective local Hubbard interactions to be used in low-energy Hamiltonians comprising the valence and conduction band states (or a subset thereof) of solids. Physically, the determination of Hubbard U corresponds to a *downfolding* procedure of the Coulomb interaction to a low-energy subspace. For the one-particle part of the Hamiltonian, downfolding techniques have been the subject of a vast literature [125, 126], and are by now well established. Downfolding of the interacting part of a many-body Hamiltonian, however, is a much less straightforward problem [127]. The challenge is an accurate description of screening of low-energy interactions by high-energy degrees of freedom. Moreover, when put this way, it also becomes obvious that the *effective bare interaction* is not just a number, but rather a function of energy. Indeed, the net result of the rearrangement of the high-energy degrees of freedom as response to a perturbation of the system is an effective reduction of the perturbation strength in the low-energy space. It is for this reason that the effective Coulomb interaction in a low-energy effective model for a correlated system is in general an order of magnitude smaller than the matrix element of the bare Coulomb interaction. Nevertheless, the latter is recovered in the limit of high-frequencies of the perturbation, when screening becomes inefficient. The crossover – as a function of frequency – from the low-energy screened regime to the high-frequency bare matrix element of $\frac{e^2}{|\mathbf{r}-\mathbf{r}'|}$ takes place at a

characteristic screening (plasma) frequency where the dielectric function exhibits a pole structure.

This frequency-dependence of the effective local Coulomb interactions, the *dynamical Hubbard* $\mathcal{U}(\omega)$ can be quantitatively assessed within the so-called "constrained random phase approximation" (cRPA) [128].[18] The cRPA provides an (approximate) answer to the following question: given the Coulomb Hamiltonian in a large Hilbert space, and a low-energy Hilbert subspace of the former, what is the effective *bare* interaction to be used in many-body calculations dealing only with the low-energy subspace in order for physical predictions for the low-energy Hilbert space to be the same for the two descriptions? With a general answer to this question not requiring much less than a full solution of the initial many-body problem, the cRPA builds on two approximations: it assumes (1) that the requirement of the same physical predictions be fulfilled as soon as in both cases the same estimate for the fully screened Coulomb interaction, Hedin's W, is obtained and (2) the validity of the random phase approximation to calculate this latter quantity.

The cRPA starts from a decomposition of the polarisation of the solid in high- and low-energy parts, where the latter is defined as given by all screening processes that are confined to the low-energy subspace. The high-energy polarisation results from all remaining screening processes:

$$P^{\text{high}} = P - P^{\text{low}}, \tag{30}$$

one then calculates a partially screened interaction

$$W^{\text{partial}}(1,2) \equiv \int d3\varepsilon^{-1}_{\text{partial}}(1,3)v(3,2), \tag{31}$$

using the *partial* dielectric function

$$\varepsilon_{\text{partial}}(1,2) = \delta(1-2) - \int d3P^{\text{high}}(1,3)v(3,2). \tag{32}$$

Here, the numbers represent space and time coordinates in a shorthand notation.

Screening W^{partial} by processes that live within the low-energy space recovers the fully screened interaction W. This justifies the interpretation of the matrix elements of W^{partial} in a localised Wannier basis as the interaction matrices to be used as bare Hubbard interactions within a low-energy effective Hubbard-like Hamiltonian written on the same Wannier basis.

Hubbard interactions – obtained as the static ($\omega = 0$) limit of $\langle |W^{\text{partial}}| \rangle$ within cRPA – have since been obtained for a variety of systems, ranging from transition

[18] In fact, the ability to determine the full frequency-dependence is probably the most important conceptual advance over traditional strategies aiming at the calculation of the static interactions only. In this category, we mention "constrained LDA" techniques, pioneered in [129, 130] as well as linear response schemes [131–133] and GW-inspired techniques [134].

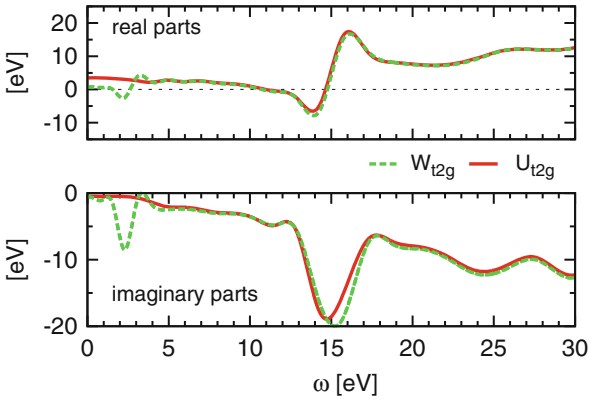

Fig. 4 Screened Coulomb interaction W and partially screened Coulomb interaction U for $SrVO_3$: ReU, ReW (*top panel*), ImU, ImW (*bottom panel*), as calculated within cRPA. Note the small low energy value of Re$U(0)$, compared to the matrix element of the bare Coulomb interaction Re$U(\infty)$, and the plasmon excitation at 15 eV. Adapted from [148]

metals [128] to oxides [135–138] (including oxides under pressure [139]), pnictides [140–143], or f-electron compounds [105], and several implementations within different electronic structure codes and basis sets exist, e.g. within linearised muffin tin orbitals [128, 135, 144], maximally localised Wannier functions [136, 145] or localised orbitals constructed from projected atomic orbitals [138]. The implementation into the framework of the Wien2k package [138] made it possible that Hubbard Us be calculated for the same orbitals as those used in subsequent LDA + DMFT calculations (see, e.g. [102]). Systematic calculations investigating the basis set dependence for a series of correlated transition metal oxides revealed furthermore interesting trends, depending on the choice of the low-energy subspace [138].

In general, values obtained within cRPA have for a long time been thought to be slightly "too small", since, quite systematically, not only do constrained LDA techniques result in larger values but also many-body calculations that fix the interactions in order to obtain agreement with experiments usually employ slightly larger values than those obtained within cRPA. This puzzle has been recently solved [146, 147]: the key was found to lie in the frequency-dependence of the interactions leading to additional renormalisations of the one-body Hamiltonian. Indeed, as can be seen from (31), $W^{\text{partial}}(\omega)$ is a function of frequency, and so are matrix elements derived from it, in particular its local part, the Hubbard $\mathcal{U}(\omega)$. An example is given in Fig. 4. The consequences of this dynamical nature of the effective interactions are the subject of the following sections.

13 Dynamical Screening Effects

The explicit treatment of many-body problems with dynamical Hubbard interactions has by now become possible even in the realistic multi-orbital case. This progress is due both to quite impressive advances in Monte Carlo techniques and to the development of extremely accurate efficient approximations that reduce the problem to a static one, at least in the anti-adiabatic limit when the characteristic screening frequencies are much larger than other relevant energy scales of the problem

(bandwidth and static Hubbard interaction $U(\omega = 0)$). Several applications to materials have appeared, namely for $SrVO_3$ in [16, 147–149], and to $BaFe_2As_2$ in [92]. As an alternative to a direct explicit treatment of the dynamical interactions, in the anti-adiabatic limit a mapping onto an effective low-energy model with static interactions can also be performed if only low-energy properties living on energy scales considerably smaller than the plasma frequency are of interest [146].

Dealing with frequency-dependent interactions at the DMFT level has also been a major bottleneck in the implementation of the combined "GW + DMFT" scheme since its proposal in 2003 [150–152]. The recent advances concerning this issue, both concerning Monte Carlo techniques and through the Bose factor ansatz, have now unblocked the situation: two calculations within GW + DMFT taking into account dynamical interactions have been achieved recently, for $SrVO_3$ [16, 148] and for systems of adatoms on surfaces [153]. Systematic studies of an extended Hubbard model [154, 155] have moreover demonstrated how the GW + DMFT scheme enables an additional type of "downfolding": effects of long-range interactions can in fact be "backfolded" into a purely local effective quantity, a generalised Hubbard $\mathcal{U}(\omega)$, which acquires its frequency-dependence due to screening by non-local processes. The strength of these screening processes was shown to be strongly system-dependent when the true long-range nature of Coulomb interactions is taken into account, while simple rules of thumb work relatively well in the case of an extended Hubbard model with nearest-neighbour interactions only.

We will start the discussion with the description of a new scheme that generalises the standard LDA + DMFT method using a static Hubbard interaction U to a scheme, where the dynamical nature of the effective local Coulomb interactions is taken into account. This method, dubbed LDA + $\mathcal{U}(\omega)$ + DMFT, can be considered as a simplified version of GW + DMFT, where non-local self-energy effects are neglected and self-consistency over two-particle quantities is omitted. We refer the interested reader to the review in [156] and the discussion in [16].

14 LDA + $\mathcal{U}$ (ω) + DMFT

Extending the philosophy of the LDA + DMFT scheme to dynamically screened interactions requires the use of a framework that allows for a description of an explicit frequency-dependence of the interactions $\mathcal{U}(\omega)$. One possibility is to switch from the Hamiltonian formulation of the "LDA++" approach to an action description where the frequency-dependent nature of the interaction is readily incorporated as a retardation in the interaction term

$$S = -\int_0^\beta \int_0^\beta \mathrm{d}\tau \mathrm{d}\tau' \mathcal{U}\left(\tau - \tau'\right) n(\tau) n\left(\tau'\right) \tag{33}$$

where we have assumed that the retarded interaction couples only to the density $n(\tau)$. Alternatively, it is possible to stick to a Hamiltonian formulation. In order to describe the retardation effects in the interaction one then needs to introduce additional bosonic degrees of freedom that parameterise the frequency dependence of the interaction. Indeed, from a physical point of view, screening can be understood as a coupling of the electrons to bosonic screening degrees of freedom such as particle-hole excitations, plasmons or more complicated composite excitations giving rise to shake-up satellites or similar features in spectroscopic probes. Mathematically, a local retarded interaction can be represented by a set of bosonic modes of frequencies ω coupling to the electronic density with strength λ_ω. The total Hamiltonian

$$H = H_{\mathrm{LDA++}} + H_{\mathrm{screening}} \tag{34}$$

is then composed by a part of "LDA++" form but with the local interactions given by the *unscreened* local matrix elements of the bare Coulomb interactions V and the Hund's exchange coupling J (assumed not to be screened by the bosons and thus frequency-independent):

$$\begin{aligned} H_{\mathrm{LDA++}} &= H^{\mathrm{KS}} + \frac{1}{2}\sum_{imm'\sigma} V^{i}_{mm'} n_{im\sigma} n_{im'-\sigma} \\ &+ \frac{1}{2}\sum_{im\neq m'\sigma} \left(V^{i}_{mm'} - J^{i}_{mm'}\right) n_{im\sigma} n_{im'\sigma} \end{aligned} \tag{35}$$

and a screening part consisting of the local bosonic modes and their coupling to the electronic density:

$$H_{\mathrm{screening}} = \sum_i \int \mathrm{d}\omega \left[\lambda_{i\omega} \left(b^{\dagger}_{i\omega} + b_{i\omega} \right) \sum_{m\sigma} n_{im\sigma} + \omega b^{\dagger}_{i\omega} b_{i\omega} \right].$$

Here, H^{KS} represents a one-body Hamiltonian defined by the DFT Kohn–Sham band structure, suitably corrected for double counting terms. As in standard LDA + DMFT, many-body interactions are included for a selected set of local "correlated" orbitals. The sums thus run over atomic sites i and correlated orbitals m centred on these sites.

Integrating out the bosonic degrees of freedom would lead back to a purely fermionic action with retarded local interactions

$$\mathcal{U}(\omega) = V + \int \mathrm{d}\omega' \lambda^2_{\omega'} \left(\frac{1}{\omega - \omega'} - \frac{1}{\omega + \omega'} \right) \tag{36}$$

The above Hamiltonian thus yields a parameterisation of the problem with frequency-dependent interactions provided that the parameters are chosen as $\mathrm{Im}\mathcal{U}(\omega) = \pi\lambda^2_\omega$.

The zero-frequency (screened) limit is then given by $U_0 = V - 2\int \mathrm{d}\omega \frac{\lambda_\omega^2}{\omega}$.

The above form of the Hamiltonian corresponds to a multi-orbital multi-mode version of the familiar Hubbard–Holstein Hamiltonian describing a system of fermions coupled to bosonic modes. The emergence of retarded interactions in the case of electron–phonon coupling has been investigated in detail for its role in the BCS theory of pairing arising in conventional superconductors. In the current situation, where the bosons represent plasmons and other screening modes, typical energy scales are radically different, and the regime of importance is most often the antiadiabatic one. Indeed, plasma frequencies of typical transition metal-based materials – transition metals themselves, their oxides, pnictides, etc. – are of the order of 15–25 eV, whereas both the typical bandwidth and static ($\omega = 0$) Hubbard interaction are rather of the order of a few eV. This hierarchy gives rise to a separation of energy scales that enables a simple and transparent physical interpretation of the solution of the Hubbard–Holstein Hamiltonian.

We illustrate this fact on the simplest example, a half-filled *single-orbital* Hubbard–Holstein model with a *single local bosonic mode* on a Bethe lattice with semi-circular density of states. The frequency ω_0 of the bosonic mode is chosen to be the largest energy scale of the problem so that the chosen parameter set places the system deep in the anti-adiabatic limit. The spectral function in this case is plotted in Fig. 5. It corresponds to a sequence of features located at energies that are positive or negative multiples of the plasma frequency. These correspond to electron removal or addition processes where the (inverse) photoemission process itself is accompanied by the creation or annihilation of a certain number of screening bosons. The low-energy part of the spectral function, close to the Fermi level – chosen to be the origin of energies – is given by electron removal or addition processes that do *not* change the number of screening bosons. In the present simple half-filled case in a moderate correlation regime, it displays a "three-peak structure", with a central quasiparticle peak and upper and lower Hubbard bands, typical of correlated metals. Interestingly, however, even this part is modified by the coupling to the bosons: indeed, since the full spectral function is normalised, spectral weight appearing in plasmon replicas of the main line reduces the weight contained in the latter. The coupling to the bosonic degrees of freedom thus leads to an additional mass renormalisation of the low-energy fermionic degrees of freedom. This effect corresponds to the mass enhancement due to the formation of "electronic polarons", fermions dressed by their screening bosons just as usual polarons can be understood as electrons dressed by the polarisation of the surrounding lattice. In the case of core level spectroscopies, such effects have been extensively discussed, and the electron–boson couplings above can be viewed as a local version of Hedin's "fluctuation potentials" (albeit, in the cRPA sense, that is parameterising not the fully screened interaction W but rather the Hubbard U) [157].

What is the relevant impurity model if we want to solve a lattice model with purely local but dynamical effective Hubbard interactions within DMFT? The

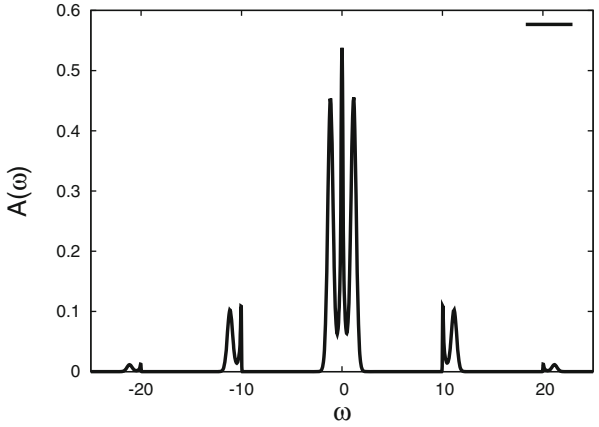

Fig. 5 Spectral function of the single-orbital single-mode Hubbard Holstein model in the anti-adiabatic limit. The chosen parameters are: a low-energy Hubbard interaction $U\,(\omega = 0) = 2$ D, a high-energy bare interaction $U\,(\omega = \infty) = 6.5$ D, and a plasma frequency of $\omega_0 = 10$ D, where D denotes the half-bandwidth of the semi-circular density of states of a Bethe lattice. The inverse temperature is $\beta D = 100$. Replicas of the low-energy part of the spectral function due to plasmon excitations are clearly seen. Adapted from [147]

answer is a straightforward generalisation of the action (13) to frequency-dependent $\mathcal{U}(\omega)$:

$$\begin{aligned} S = &-\int\int \mathrm{d}\tau \mathrm{d}\tau' \sum_{\sigma} c^{\dagger}(\tau')\left(\delta(\tau-\tau')\partial_{\tau} - \Delta(\tau-\tau')\right)c(\tau) \\ &+\int\int \mathrm{d}\tau \mathrm{d}\tau' \mathcal{U}(\tau-\tau')n(\tau)n(\tau') \end{aligned} \tag{37}$$

where $n(\tau) = n_{\uparrow}(\tau) + n_{\downarrow}(\tau)$.

An extremely efficient scheme for the solution of this problem, suitable in the anti-adiabatic regime, is the recently introduced [147] "Boson factor ansatz" (BFA). It approximates the local Green's function of the dynamical impurity model as follows:

$$G(\tau) = -\left\langle \mathcal{T}\, c(\tau)c^{\dagger}(0)\right\rangle = \left(\frac{G(\tau)}{G_{\mathrm{stat}}(\tau)}\right) G_{\mathrm{stat}}(\tau)^{\sim} \left(\frac{G(\tau)}{G_{\mathrm{stat}}(\tau)}\right)\Bigg|_{\Delta=0} G_{\mathrm{stat}}(\tau) \tag{38}$$

where G_{stat} is the Green's function of a fully interacting impurity model with *purely static interaction* $U = U(\omega = 0)$, and the first factor is approximated by its value for vanishing bath hybridisation Δ [147]. In this case, it can be analytically evaluated in terms of the frequency-dependent interaction:

$$B(\tau) = \left(\frac{G(\tau)}{G_{\text{stat}}(\tau)}\right)\Big|_{\Delta=0} = \mathrm{e}^{-\int_0^\infty \frac{\mathrm{d}\omega}{\pi} \frac{\mathrm{Im}U(\omega)}{\omega^2}(K_\tau(\omega)-K_0(\omega))} \tag{39}$$

with $K_\tau(\omega) = \frac{\exp(-\tau\omega)+\exp(-(\beta-\tau)\omega)}{1-\exp(-\beta\omega)}$. In the regime that we are interested in, namely when the plasma frequency that characterises the variation of U from the partially screened to the bare value is typically several times the bandwidth, this is an excellent approximation, as was verified by benchmarks against direct Monte Carlo calculations in [147]. The reason can be understood when considering the solution of the dynamical local model in the *dynamical atomic limit* $\Delta = 0$, that is, when there are no hopping processes possible between the impurity site and the bath. In this case the BFA trivially yields the exact solution, and the factorisation can be understood as a factorisation into a Green's function determined by the static Fourier component of $\mathcal{U}$ only, and the exponential factor B which only depends on the non-zero frequency components of $\mathcal{U}$. The former fully determines the low-energy spectral function of the problem, while the latter is responsible for generating high-energy replicas of the low-energy spectrum. For finite bath hybridisation, the approximation consists of assuming that the factorisation still holds and that the finite bath hybridisation modifies only the low-energy static-U Green's function, leaving the general structure of the plasmon replica generation untouched. The approximation thus relies on the energy scale separation between low-energy processes and plasmon energy; it becomes trivially exact not only in the atomic limit but also in the static limit given by small electron–boson couplings or large plasmon energy.

The BFA lends a precise mathematical meaning to the physical discussion of the generation of plasmon replicas. Indeed, the factorisation of the Green's function corresponds in frequency space to a convolution of the spectral representations of the low-energy Green's function G_{static} and the bosonic factor B. In terms of the spectral function $A_{\text{stat}}(\omega)$ of the static Green's function $G_{\text{stat}}(\omega)$ and the (bosonic) spectral function $B\ (\varepsilon)$ of the bosonic factor $B\ (\tau)$ defined above, the spectral function $A\ (\omega)$ of the full Green's function $G(\tau)$ reads

$$A\,(\omega) = \int_{-\infty}^{\infty} \mathrm{d}\varepsilon\, B\,(\varepsilon)\, \frac{1+\mathrm{e}^{-\beta\omega}}{(1+\mathrm{e}^{-\beta(\varepsilon-\omega)})(1-\mathrm{e}^{-\beta\varepsilon})} A_{\text{stat}}(\omega-\varepsilon). \tag{40}$$

In the case of a single mode of frequency ω_0, the bosonic spectral function consists of sharp peaks at energies given by that frequency, and the convolution generates replicas of the spectral function $A_{\text{stat}}(\omega)$ of the static part. Due to the overall normalisation of the spectral function, the appearance of replica satellites is necessarily accompanied by a transfer of spectral weight to high energies. This mechanism induces a corresponding loss of spectral weight in the low-energy part of the spectral function. Indeed, it can be shown [146] that the spectral weight

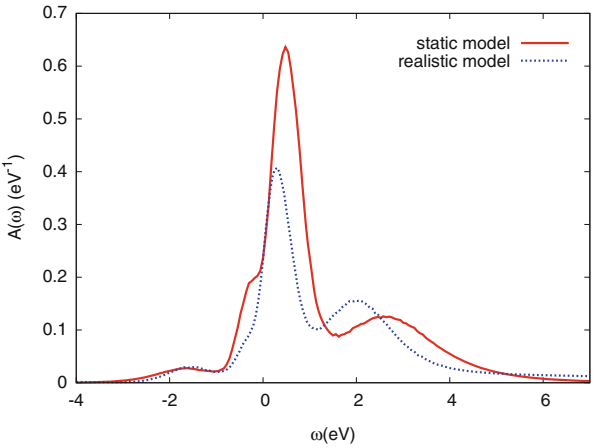

Fig. 6 Spectral function of a low-energy (t_{2g}-only) Hamiltonian within "LDA + $\mathcal{U}(\omega)$ + DMFT" as compared to a standard LDA + DMFT calculation with static interactions; see text. Adapted from [147]

corresponding to the low-energy part as defined by a projection on zero boson states is reduced by the factor

$$Z_B = \exp\left(-1/\pi \int_0^\infty \mathrm{d}\nu \ \mathrm{Im}\mathcal{U}(\nu)/\nu^2\right). \tag{41}$$

Estimates of Z_B for typical transition metal oxides vary between 0.5 and 0.9, depending on the energy scale of the plasma frequency and the efficiency of screening (as measured, e.g. by the difference between bare Coulomb interaction $\left\langle \left| \frac{1}{|r-r'|} \right| \right\rangle = \mathcal{U}(\omega = \infty)$ and the static value $\mathcal{U}(\omega = 0)$).

We reproduce in Fig. 6 the low-energy spectral function of an "LDA + $\mathbf{U}(\omega)$ + DMFT" calculation for the d^1 ternary transition metal perovskite $SrVO_3$, demonstrating the reduction of spectral weight compared to a static-U calculation [146]. It should be noted, however, that the calculation included the t_{2g} states only. The contribution of unoccupied e_g states dominates at energies as low as ~2.5 eV. Also, non-local self-energy effects stemming from screened exchange interactions are non-negligible in this compound and alter the unoccupied part of the t_{2g} spectrum quite considerably. This was recently discussed in the context of the very first dynamical implementation of the combined GW + DMFT scheme and its application to $SrVO_3$ [16, 148].

15 Conclusions and Perspectives

We have given an introduction to dynamical mean field-based approaches to the spectroscopy of *correlated materials*. Starting from the necessity of *going beyond the single-particle picture* of band theory, we have traced the developments of DMFT-based many-body theory for correlated solids from the most simple

fermionic lattice model up to recent developments in going beyond the established LDA + DMFT scheme.

LDA + DMFT-based electronic structure calculations have – over the last 15 years – helped to elucidate physical phenomena in a variety of correlated materials ranging from transition metal oxides and sulphides, *f*-electron compounds and iron pnictides to organic materials. Three examples have been described in the chapter.

We have also tried to convey to the reader the efforts being made in pushing the frontiers further; the struggle to make DMFT-based techniques truly predictive goes hand in hand with the development of techniques for assessing the effective Coulomb interactions. Recent cRPA techniques are a big leap forward in that they allow for a probably quite accurate albeit approximate "downfolding" of the interactions to the low-energy subspaces actually dealt with in practical calculations. Open questions nevertheless persist when these subspaces are entangled with further "itinerant states", when ligand orbitals interact and hybridise with "correlated states" or when non-local interactions and correlations cannot be neglected.

We have explained in detail how screening by "downfolded" higher-energy degrees of freedom leads to effective dynamical interactions. Interestingly, these not only determine the interaction part of the Hamiltonian but also renormalise the kinetic energy, emphasising that one cannot be treated without the other. This observation calls for functional-based approaches, beyond simple combinations of tight-binding Hamiltonians with Hubbard parameters. Recent progress in combined GW + DMFT techniques [16, 148, 153] is a promising step in the right direction. At the same time, it is also clear that there is still some way to go until first-principles many-body techniques will have realised their full predictive potential, suitable to serve materials scientists in designing new unknown materials. While progress is rapid, the field is nevertheless likely to remain alive and kicking for a while.

Acknowledgements My view on the field, and specifically on the work summarised here, has been influenced over the years by discussions and collaborations with numerous colleagues. I thank in particular M. Aichhorn, F. Aryasetiawan, M. Casula, M. Ferrero, A. Georges, M. Katsnelson, F. Lechermann, A.I. Lichtenstein, C. Martins, O. Parcollet, L. Pourovskii, A. Rubtsov, J.M. Tomczak, L. Vaugier and V. Vildosola most warmly for the fruitful and enjoyable collaborations. I also thank P. Seth for her careful reading of the manuscript.

This work was supported by the French ANR under projects SURMOTT and PNICTIDES, and IDRIS/GENCI under project 139313.

References

1. Alloul H (2010) Physics of electrons in solids. Springer, New York
2. Kotani T (2000) Ab initio random-phase-approximation calculation of the frequency-dependent effective interaction between 3d electrons: Ni, Fe, and MnO. J Phys Condens Matter 12(7):2413
3. Springer M, Aryasetiawan F (1998) Frequency-dependent screened interaction in Ni within the random-phase approximation. Phys Rev B 57(8):4364–4368
4. Yoshida T, Tanaka K, Yagi H, Ino A, Eisaki H, Fujimori A, Shen Z-X (2005) Direct observation of the mass renormalization in SrVO3. Phys Rev Lett 95:146404

5. Georges A, Florens S, Costi TA (2004) A brief review of recent advances on the Mott transition: unconventional transport, spectral weight transfers, and critical behaviour. J Phys IV 114:165
6. Imada M, Fujimori A, Tokura Y (1998) Metal–insulator transitions. Rev Mod Phys 70 (4):1039–1263
7. Greenberg CB (1983) Thermochromic vanadium oxide with depressed switching temperature. US patent 4401690
8. Li S-Y, Niklasson GA, Granqvist CG (2012) Thermochromic fenestration with vo_2-based materials: three challenges and how they can be met. Thin Solid Films 520(10):3823–3828
9. Tomczak JM, Biermann S (2009) Materials design using correlated oxides: optical properties of vanadium dioxide. Europhys Lett 86(3):37004
10. Tomczak JM, Biermann S (2009) Optical properties of correlated materials – or why intelligent windows may look dirty. Phys Status Solidi B (feature article), 246(9):1996. Scientific Highlight of the Month of the Ψk Network, no. 88, Aug 2008
11. Anisimov VI, Aryasetiawan F, Lichtenstein AI (1997) First-principles calculations of the electronic structure and spectra of strongly correlated systems: the LDA+U method. J Phys Condens Matter 9(4):767
12. Tomczak JM, Haule K, Kotliar G (2012) Signatures of electronic correlations in iron silicide. Proc Natl Acad Sci U S A 109(9):3243–3246
13. Hohenberg P, Kohn W (1964) Inhomogeneous electron gas. Phys Rev 136(3B):B864–B871
14. Kohn W (1999) Nobel lecture: electronic structure of matter-wave functions and density functionals. Rev Mod Phys 71(5):1253–1266
15. Kohn W, Sham LJ (1965) Self-consistent equations including exchange and correlation effects. Phys Rev 140(4A):A1133–A1138
16. Tomczak JM, Casula M, Miyake T, Biermann S (2013) Asymmetric band widening by screened exchange competing with local correlations in SrVO3: new surprises on an old compound from combined GW and dynamical mean field theory GW+DMFT PRB. Submitted arxiv1312.7546
17. Mott N (1961) The transition to the metallic state. Phil Mag 6:287
18. Gutzwiller MC (1963) Effect of correlation on the ferromagnetism of transition metals. Phys Rev Lett 10(5):159–162
19. Gutzwiller MC (1965) Correlation of electrons in a narrow *s* band. Phys Rev 137(6A): A1726–A1735
20. Hubbard J (1963) Electron correlations in narrow energy bands. R Soc Lond Proc A 276:238–257
21. Hubbard J (1964) Electron correlations in narrow energy bands. III. An improved solution. R Soc Lond Proc A 281:401–419
22. Kanamori J (1963) Electron correlation and ferromagnetism of transition metals. Progr Theor Phys 30(3):275–289
23. Metzner W, Vollhardt D (1989) Correlated lattice fermions in $d = \infty$ dimensions. Phys Rev Lett 62(3):324–327
24. Georges A, Kotliar G, Krauth W, Rozenberg MJ (1996) Dynamical mean-field theory of strongly correlated fermion systems and the limit of infinite dimensions. Rev Mod Phys 68(1):13
25. Pruschke T, Jarrell M, Freericks JK (1995) Anomalous normal-state properties of high-Tc superconductors: intrinsic properties of strongly correlated electron systems? Adv Phys 44 (2):187
26. Vollhardt D (1991) Investigation of correlated electron systems using the limit of high dimensions. Lecture-notes for the 9th Jerusalem Winter School for Theoretical Physics, Jerusalem 30. Dec 1991–8. Jan 1992. Emery VJ (World Scientific, Singapore), Dec 1991
27. Gull E, Millis AJ, Lichtenstein AI, Rubtsov AN, Troyer M, Werner P (2011) Continuous-time Monte Carlo methods for quantum impurity models. Rev Mod Phys 83:349–404
28. Lichtenstein AI, Katsnelson MI (1998) Ab initio calculations of quasiparticle band structure in correlated systems: LDA++ approach. Phys Rev B 57(12):6884–6895

29. Anisimov VI, Poteryaev AI, Korotin MA, Anokhin AO, Kotliar G (1997) First-principles calculations of the electronic structure and spectra of strongly correlated systems: dynamical mean-field theory. J Phys Condens Matter 9(35):7359–7367
30. Lechermann F, Georges A, Poteryaev A, Biermann S, Posternak M, Yamasaki A, Andersen OK (2006) Dynamical mean-field theory using Wannier functions: a flexible route to electronic structure calculations of strongly correlated materials. Phys Rev B 74(12):125120
31. Anisimov VI, Kondakov DE, Kozhevnikov AV, Nekrasov IA, Pchelkina ZV, Allen JW, Mo S-K, Kim H-D, Metcalf P, Suga S, Sekiyama A, Keller G, Leonov I, Ren X, Vollhardt D (2005) Full orbital calculation scheme for materials with strongly correlated electrons. Phys Rev B 71(12):125119
32. Pourovskii LV, Amadon B, Biermann S, Georges A (2007) Self-consistency over the charge density in dynamical mean-field theory: a linear muffin-tin implementation and some physical implications. Phys Rev B 76(23):235101
33. Savrasov SY, Kotliar G, Abrahams E (2001) Correlated electrons in δ-plutonium within a dynamical mean-field picture. Nature 410(6830):793
34. Minár J, Chioncel L, Perlov A, Ebert H, Katsnelson MI, Lichtenstein AI (2005) Multiple-scattering formalism for correlated systems: a KKR-DMFT approach. Phys Rev B 72(4):045125
35. Biermann S, Dallmeyer A, Carbone C, Eberhardt W, Pampuch C, Rader O, Katsnelson MI, Lichtenstein AI (2004) Observation of Hubbard bands in gamma-manganese. JETP Lett 80 (9):612
36. Biermann S (2000) Neuartige Ansätze zur Behandlung des Vielteilchenproblems in kondensierter Materie. PhD thesis, Universität Köln
37. Lichtenstein AI, Katsnelson MI, Kotliar G (2001) Finite-temperature magnetism of transition metals: an ab initio dynamical mean-field theory. Phys Rev Lett 87:067205
38. Augustinský P, Křápek V, Kuneš J (2013) Doping induced spin state transition in $LaCoO_3$: dynamical mean-field study. Phys Rev Lett 110:267204
39. De Raychaudhury M, Pavarini E, Andersen OK (2007) Orbital fluctuations in the different phases of $LaVO_3$ and YVO_3. Phys Rev Lett 99:126402
40. Flesch A, Zhang G, Koch E, Pavarini E (2012) Orbital-order melting in rare-earth manganites: role of superexchange. Phys Rev B 85:035124
41. Gorelov E, Karolak M, Wehling TO, Lechermann F, Lichtenstein AI, Pavarini E (2010) Nature of the Mott transition in Ca_2RuO_4. Phys Rev Lett 104:226401
42. Hansmann P, Haverkort MW, Toschi A, Sangiovanni G, Rodolakis F, Rueff JP, Marsi M, Held K (2012) Atomic and itinerant effects at the transition-metal X-ray absorption *k* pre-edge exemplified in the case of V_2O_3. Phys Rev B 85:115136
43. Held K, Keller G, Eyert V, Vollhardt D, Anisimov VI (2001) Mott-Hubbard metal–insulator transition in paramagnetic V_2O_3: an *LDA + DMFT(QMC)* study. Phys Rev Lett 86(23):5345–5348
44. Keller G, Held K, Eyert V, Vollhardt D, Anisimov VI (2004) Electronic structure of paramagnetic V_2O_3: strongly correlated metallic and Mott insulating phase. Phys Rev B 70(20):205116
45. Kuneš J, Korotin DM, Korotin MA, Anisimov VI, Werner P (2009) Pressure-driven metal–insulator transition in hematite from dynamical mean-field theory. Phys Rev Lett 102:146402
46. Liebsch A (2003) Surface versus bulk coulomb correlations in photoemission spectra of $SrVO_3$ and $CaVO_3$. Phys Rev Lett 90(9):096401
47. Nekrasov IA, Held K, Keller G, Kondakov DE, Pruschke T, Kollar M, Andersen OK, Anisimov VI, Vollhardt D (2006) Momentum-resolved spectral functions of SrVO3 calculated by LDA + DMFT. Phys Rev B 73(15):155112
48. Nekrasov IA, Keller G, Kondakov DE, Kozhevnikov AV, Pruschke T, Held K, Vollhardt D, Anisimov VI (2005) Comparative study of correlation effects in CaVO3 and SrVO3. Phys Rev B 72:155106
49. Pavarini E, Biermann S, Poteryaev A, Lichtenstein AI, Georges A, Andersen OK (2004) Mott transition and suppression of orbital fluctuations in orthorhombic 3d1 perovskites. Phys Rev Lett 92(17):176403
50. Pavarini E, Koch E (2010) Origin of Jahn-Teller distortion and orbital order in $LaMnO_3$. Phys Rev Lett 104:086402

51. Poteryaev AI, Tomczak JM, Biermann S, Georges A, Lichtenstein AI, Rubtsov AN, Saha-Dasgupta T, Andersen OK (2007) Enhanced crystal-field splitting and orbital-selective coherence induced by strong correlations in V2O3. Phys Rev B 76(8):085127
52. Rodolakis F, Hansmann P, Rueff J-P, Toschi A, Haverkort MW, Sangiovanni G, Tanaka A, Saha-Dasgupta T, Andersen OK, Held K, Sikora M, Alliot I, Itié J-P, Baudelet F, Wzietek P, Metcalf P, Marsi M (2010) Inequivalent routes across the Mott transition in V_2O_3 explored by X-ray absorption. Phys Rev Lett 104:047401
53. Saha-Dasgupta T, Lichtenstein A, Valentí R (2005) Correlation effects on the electronic structure of TiOCl: a NMTO + DMFT study. Phys Rev B 71:153108
54. Tomczak JM, Biermann S (2009) Multi-orbital effects in optical properties of vanadium sesquioxide. J Phys Condens Matter 21(064209)
55. Wang X, Han MJ, de' Medici L, Park H, Marianetti CA, Millis AJ (2012) Covalency, double-counting, and the metal–insulator phase diagram in transition metal oxides. Phys Rev B 86:195136
56. Zhang G, Gorelov E, Koch E, Pavarini E (2012) Importance of exchange anisotropy and superexchange for the spin-state transitions in RCoO3 (R = rare earth) cobaltates. Phys Rev B 86:184413
57. Lechermann F, Biermann S, Georges A (2005) Importance of interorbital charge transfers for the metal-to-insulator transition of BaVS3. Phys Rev Lett 94(16):166402
58. Lechermann F, Biermann S, Georges A (2007) Competing itinerant and localized states in strongly correlated $BaVS_3$. Phys Rev B 76(8):085101
59. Amadon B, Biermann S, Georges A, Aryasetiawan F (2006) The alpha-gamma transition of cerium is entropy driven. Phys Rev Lett 96(6):066402
60. Held K, McMahan AK, Scalettar RT (2001) Cerium volume collapse: results from the merger of dynamical mean-field theory and local density approximation. Phys Rev Lett 87 (27):276404
61. Shim JH, Haule K, Savrasov S, Kotliar G (2008) Screening of magnetic moments in PuAm alloy: local density approximation and dynamical mean field theory study. Phys Rev Lett 101:126403
62. Zölfl MB, Nekrasov IA, Pruschke T, Anisimov VI, Keller J (2001) Spectral and magnetic properties of α- and γ-Ce from dynamical mean-field theory and local density approximation. Phys Rev Lett 87(27):276403
63. Aichhorn M, Biermann S, Miyake T, Georges A, Imada M (2010) Theoretical evidence for strong correlations and incoherent metallic state in FeSe. Phys Rev B 82:064504
64. Aichhorn M, Pourovskii L, Vildosola V, Ferrero M, Parcollet O, Miyake T, Georges A, Biermann S (2009) Dynamical mean-field theory within an augmented plane-wave framework: assessing electronic correlations in the iron pnictide LaFeAsO. Phys Rev B 80:085101
65. Anisimov VI, Korotin DM, Korotin MA, Kozhevnikov AV, Kunes J, Shorikov AO, Skornyakov SL, Streltsov SV (2009) Coulomb repulsion and correlation strength in LaFeAsO from density functional and dynamical mean-field theories. J Phys Condens Matter 21(7):075602
66. Ferber J, Foyevtsova K, Valentí R, Jeschke HO (2012) LDA + DMFT study of the effects of correlation in LiFeAs. Phys Rev B 85:094505
67. Hansmann P, Arita R, Toschi A, Sakai S, Sangiovanni G, Held K (2010) Dichotomy between large local and small ordered magnetic moments in iron-based superconductors. Phys Rev Lett 104:197002
68. Haule K, Shim JH, Kotliar G (2008) Correlated electronic structure of LaO1−xFxFeAs. Phys Rev Lett 100:226402
69. Lee H, Zhang Y-Z, Jeschke HO, Valentí R (2010) Possible origin of the reduced ordered magnetic moment in iron pnictides: a dynamical mean-field theory study. Phys Rev B 81:220506
70. Skornyakov SL, Efremov AV, Skorikov NA, Korotin MA, YuIzyumov YA, Anisimov VI, Kozhevnikov AV, Vollhardt D (2009) Classification of the electronic correlation strength in the iron pnictides: the case of the parent compound $BaFe_2As_2$. Phys Rev B 80:092501
71. Ruff A, Sing M, Claessen R, Lee H, Tomić M, Jeschke HO, Valentí R (2013) Absence of metallicity in K-doped picene: importance of electronic correlations. Phys Rev Lett 110:216403

72. Arita R, Kuroki K, Held K, Lukoyanov AV, Skornyakov S, Anisimov VI (2008) Origin of large thermopower in $LiRh_2O_4$: calculation of the Seebeck coefficient by the combination of local density approximation and dynamical mean-field theory. Phys Rev B 78(11):115121
73. Held K, Arita R, Anisimov VI, Kuroki K (2009) The LDA+DMFT route to identify good thermoelectrics. In: Zlatic V, Hewson AC (eds) Properties and applications of thermoelectric materials, NATO Science for Peace and Security Series B: Physics and Biophysics. Springer, Amsterdam, pp 141–157. doi:10.1007/978-90-481-2892-1_9
74. Weber C, O'Regan DD, Hine NDM, Littlewood PB, Kotliar G, Payne MC (2013) Importance of many-body effects in the kernel of hemoglobin for ligand binding. Phys Rev Lett 110:106402
75. Han MJ, Wang X, Marianetti CA, Millis AJ (2011) Dynamical mean-field theory of nickelate superlattices. Phys Rev Lett 107:206804
76. Hansmann P, Toschi A, Yang X, Andersen OK, Held K (2010) Electronic structure of nickelates: from two-dimensional heterostructures to three-dimensional bulk materials. Phys Rev B 82:235123
77. Lechermann F, Boehnke L, Grieger D (2013) Formation of orbital-selective electron states in $LaTiO_3/SrTiO_3$ superlattices. Phys Rev B 87:241101
78. Kotliar G, Savrasov SY, Haule K, Oudovenko VS, Parcollet O, Marianetti CA (2006) Electronic structure calculations with dynamical mean-field theory. Rev Mod Phys 78 (3):865–951
79. Anisimov VI (2000) Strong coulomb correlations in electronic structure calculations: beyond the local density approximation. Gordon and Breach Science Publishers, Amsterdam
80. Biermann S (2006) Electronic structure of transition metal compounds: DFT-DMFT approach. In: Buschow KHJ, Cahn RW, Flemings MC, Ilschner B, Kramer EJ, Mahajan S, Veyssire P (eds) Encyclopedia of materials: science and technology. Elsevier, Oxford, pp 1–9
81. Held K, Nekrasov IA, Keller G, Eyert V, Blümer N, McMahan AK, Scalettar RT, Pruschke T, Anisimov VI, Vollhardt D (2003) Realistic investigations of correlated electron systems within LDA+DMFT. Phys Status Solid (B), 243(2599), 2006. Psi-k Newsl 56 (65) 2003
82. Kotliar G, Vollhardt D (2004) Strongly correlated materials: insights from dynamical mean-field theory. Phys Today 57(3):53
83. Tomczak JM, Poteryaev AI, Biermann S (2009) Momentum-resolved spectroscopy of correlated metals: a view from dynamical mean field theory. Compt Rend Phys 10(6):537–547
84. Braun J, Minár J, Ebert H, Katsnelson MI, Lichtenstein AI (2006) Spectral function of ferromagnetic 3d metals: a self-consistent LSDA + DMFT approach combined with the one-step model of photoemission. Phys Rev Lett 97(22):227601
85. Grechnev A, Di Marco I, Katsnelson MI, Lichtenstein AI, Wills J, Eriksson O (2007) Theory of bulk and surface quasiparticle spectra for Fe, Co, and Ni. Phys Rev B 76:035107
86. Kolorenč J, Poteryaev AI, Lichtenstein AI (2012) Valence-band satellite in ferromagnetic nickel: LDA+DMFT study with exact diagonalization. Phys Rev B 85:235136
87. Sánchez-Barriga J, Braun J, Minár J, Di Marco I, Varykhalov A, Rader O, Boni V, Bellini V, Manghi F, Ebert H, Katsnelson MI, Lichtenstein AI, Eriksson O, Eberhardt W, Dürr HA, Fink J (2012) Effects of spin-dependent quasiparticle renormalization in Fe, Co, and Ni photoemission spectra: an experimental and theoretical study. Phys Rev B 85:205109
88. Sánchez-Barriga J, Fink J, Boni V, Di Marco I, Braun J, Minár J, Varykhalov A, Rader O, Bellini V, Manghi F, Ebert H, Katsnelson MI, Lichtenstein AI, Eriksson O, Eberhardt W, Dürr HA (2009) Strength of correlation effects in the electronic structure of iron. Phys Rev Lett 103:267203
89. Sánchez-Barriga J, Minár J, Braun J, Varykhalov A, Boni V, Di Marco I, Rader O, Bellini V, Manghi F, Ebert H, Katsnelson MI, Lichtenstein AI, Eriksson O, Eberhardt W, Dürr HA, Fink J (2010) Quantitative determination of spin-dependent quasiparticle lifetimes and electronic correlations in HCP cobalt. Phys Rev B 82:104414
90. Gazzara CP, Middleton RM, Weiss RJ, Hall EO (1967) A refinement of the parameters of a manganese. Acta Crystallogr 22:859

91. Medici L, Mravlje J, Georges A (2011) Janus-faced influence of Hund's rule coupling in strongly correlated materials. Phys Rev Lett 107:256401
92. Werner P, Casula M, Miyake T, Aryasetiawan F, Millis AJ, Biermann S (2012) Satellites and large doping and temperature dependence of electronic properties in hole-doped BaFe2As2. Nat Phys 8:331–337
93. Di Marco I, Minár J, Chadov S, Katsnelson MI, Ebert H, Lichtenstein AI (2009) Correlation effects in the total energy, the bulk modulus, and the lattice constant of a transition metal: combined local-density approximation and dynamical mean-field theory applied to Ni and Mn. Phys Rev B 79:115111
94. Di Marco I, Minár J, Braun J, Katsnelson MI, Grechnev A, Ebert H, Lichtenstein AI, Eriksson O (2009) γ-Mn at the border between weak and strong correlations. Eur Phys J B 72(4):473–478
95. Florens S, Georges A, Kotliar G, Parcollet O (2002) Mott transition at large orbital degeneracy: dynamical mean-field theory. Phys Rev B 66:205102
96. Cao G, Bolivar J, McCall S, Crow JE, Guertin RP (1998) Weak ferromagnetism, metal-to-nonmetal transition, and negative differential resistivity in single-crystal Sr_2IrOs_4. Phys Rev B 57(18), R11039
97. Arita R, Kuneš J, Kozhevnikov AV, Eguiluz AG, Imada M (2012) Ab initio studies on the interplay between spin-orbit interaction and coulomb correlation in Sr_2IrO_4 and Ba_2IrO_4. Phys Rev Lett 108:086403
98. Jin H, Jeong H, Ozaki T, Yu J (2009) Anisotropic exchange interactions of spin-orbit-integrated states in Sr_2IrO_4. Phys Rev B 80(7):075112
99. Kim BJ, Hosub Jin SJ, Moon J-Y, Kim B-G, Park CS, Leem JY, Noh TW, Kim C, Oh S-J, Park J-H, Durairaj V, Cao G, Rotenberg E (2008) Novel $J_{eff} = 1/2$ Mott state induced by relativistic spin-orbit coupling in Sr2IrO4. Phys Rev Lett 101(7):076402
100. Kim BJ, Ohsumi H, Komesu T, Sakai S, Morita T, Takagi H, Arima T (2009) Phase-sensitive observation of a spin-orbital Mott state in Sr2IrO4. Science 323(5919):1329
101. Watanabe H, Shirakawa T, Yunoki S (2010) Microscopic study of a spin-orbit-induced Mott insulator in Ir oxides. Phys Rev Lett 105(21):216410
102. Martins C, Aichhorn M, Vaugier L, Biermann S (2011) Reduced effective spin-orbital degeneracy and spin-orbital ordering in paramagnetic transition-metal oxides: Sr_2IrO_4 versus Sr_2RhO_4. Phys Rev Lett 107:266404
103. Moon SJ, Jin H, Choi WS, Lee JS, Seo SSA, Yu J, Cao G, Noh TW, Lee YS (2009) Temperature dependence of the electronic structure of the $J_{eff} = 1/2$ Mott insulator Sr2IrO4 studied by optical spectroscopy. Phys Rev B 80(19):195110
104. Poyurovskii L, Vildosola V, Biermann S, Georges A (2008) Local moment behavior versus Kondo behavior of the 4f-electrons in rare-earth iron oxypnictides. Europhys Lett 84:37006
105. Tomczak JM, Pourovskii LV, Vaugier L, Georges A, Biermann S (2012) Colours from first-principles: heavy-metal vs. rare-earth pigments. Submitted
106. Karolak M, Ulm G, Wehling TO, Mazurenko V, Poteryaev A, Lichtenstein Double AI (2010) Counting in LDA+DMFT – the example of NiO. J Electron Spectr Relat Phenom 181(1):11–15
107. Maier T, Jarrell M, Pruschke T, Hettler MH (2005) Quantum cluster theories. Rev Mod Phys 77:1027–1080
108. Biermann S, Poteryaev A, Lichtenstein AI, Georges A (2005) Dynamical singlets and correlation-assisted Peierls transition in VO_2. Phys Rev Lett 94(2):026404
109. Mazurenko VV, Lichtenstein AI, Katsnelson MI, Dasgupta I, Saha-Dasgupta T, Anisimov VI (2002) Nature of insulating state in NaV_2O_5 above charge-ordering transition: a cluster dynamical mean-field study. Phys Rev B 66:081104
110. Poteryaev AI, Lichtenstein AI, Kotliar G (2004) Nonlocal coulomb interactions and metal–insulator transition in Ti_2O_3: a cluster LDA + DMFT approach. Phys Rev Lett 93:086401
111. Berthod C, Giamarchi T, Biermann S, Georges A (2006) Breakup of the fermi surface near the Mott transition in low-dimensional systems. Phys Rev Lett 97(13):136401
112. Biermann S, Georges A, Lichtenstein A, Giamarchi T (2001) Deconfinement transition and Luttinger to Fermi liquid crossover in quasi-one-dimensional systems. Phys Rev Lett 87 (27):276405

113. Biermann S, Georges A, Lichtenstein A, Giamarchi T (2002) Quasi-one-dimensional organic conductors: dimensional crossover and some puzzles. In: Lerner IV et al (eds) Strongly correlated fermions and bosons in low-dimensional and disordered systems. Kluwer, Dordrecht, p 035312
114. Giamarchi T, Biermann S, Georges A, Lichtenstein AI (2004) Dimensional crossover and deconfinement in Bechgaard salts. J Phys IV France 114:23
115. Laad MS, Craco L, Müller-Hartmann E (2005) VO_2: a two-fluid incoherent metal? Europhys Lett 69(6):984–989
116. Liebsch A, Ishida H, Bihlmayer G (2005) Coulomb correlations and orbital polarization in the metal–insulator transition of VO_2. Phys Rev B 71(8):085109
117. Tomczak JM, Biermann S (2007) Effective band structure of correlated materials: the case of VO2. J Phys Condens Matter 19(36):365206
118. Tomczak JM, Aryasetiawan F, Biermann S (2008) Effective bandstructure in the insulating phase versus strong dynamical correlations in metallic VO2. Phys Rev B 78(11):115103
119. Tomczak JM, Biermann S (2009) Optical properties of correlated materials: generalized Peierls approach and its application to VO2. Phys Rev B 80(8):085117
120. Sangiovanni G, Toschi A, Koch E, Held K, Capone M, Castellani C, Gunnarsson O, Mo S-K, Allen JW, Kim H-D, Sekiyama A, Yamasaki A, Suga PS (2006) Metcalf static vs. dynamical mean field theory of Mott antiferromagnets. Phys Rev B 73:205121
121. Chantis AN, van Schilfgaarde M, Kotani T (2007) GW method applied to localized 4f electron systems. Phys Rev B 76:165126
122. Jiang H, Gomez-Abal RI, Rinke P, Scheffler M (2009) Localized and itinerant states in lanthanide oxides united by GW@LDA+U. Phys Rev Lett 102:126403
123. Hong J, Ricardo G-A, Patrick R, Matthias S (2010) First-principles modeling of localized *d* states with the GW@LDA+U approach. Phys Rev B 82:045108
124. Hong J, Patrick R, Matthias S (2012) Electronic properties of lanthanide oxides from the *GW* perspective. Phys Rev B 86:125115
125. Löwdin P-O (1951) A note on the quantum-mechanical perturbation theory. J Chem Phys 19 (11):1396
126. Saha-Dasgupta T, Andersen OK, Poteryaev A (2007) Wannier orbitals and first-principles modeling of V_2O_3: an NMTO study (unpublished)
127. Aryasetiawan F, Tomczak JM, Miyake T, Sakuma R (2009) Downfolded self-energy of many-electron systems. Phys Rev Lett 102(17):176402
128. Aryasetiawan F, Imada M, Georges A, Kotliar G, Biermann S, Lichtenstein AI (2004) Frequency-dependent local interactions and low-energy effective models from electronic structure calculations. Phys Rev B 70(19):195104
129. Anisimov VI, Gunnarsson O (1991) Density-functional calculation of effective coulomb interactions in metals. Phys Rev B 43:7570–7574
130. Dederichs PH, Blügel S, Zeller R, Akai H (1984) Ground states of constrained systems: application to cerium impurities. Phys Rev Lett 53:2512–2515
131. Cococcioni M (2002) A LDA+U study of selected iron compounds. PhD thesis, Trieste
132. Cococcioni M, de Gironcoli S (2005) Linear response approach to the calculation of the effective interaction parameters in the LDA + U method. Phys Rev B 71(3):035105
133. Pickett WE, Erwin SC, Ethridge EC (1998) Reformulation of the LDA + *u* method for a local-orbital basis. Phys Rev B 58:1201–1209
134. Kutepov A, Haule K, Savrasov SY, Kotliar G (2010) Self-consistent *GW* determination of the interaction strength: application to the iron arsenide superconductors. Phys Rev B 82:045105
135. Aryasetiawan F, Karlsson K, Jepsen O, Schönberger U (2006) Calculations of Hubbard *u* from first-principles. Phys Rev B 74:125106
136. Miyake T, Aryasetiawan F (2008) Screened coulomb interaction in the maximally localized Wannier basis. Phys Rev B 77(8):085122
137. Tomczak JM, Miyake T, Aryasetiawan F (2010) Realistic many-body models for manganese monoxide under pressure. Phys Rev B 81(11):115116

138. Vaugier L, Jiang H, Biermann S (2012) Hubbard *u* and Hund exchange *j* in transition metal oxides: screening versus localization trends from constrained random phase approximation. Phys Rev B 86:165105
139. Tomczak JM, Miyake T, Sakuma R, Aryasetiawan F (2009) Effective Coulomb interactions in solids under pressure. Phys Rev B 79(23):235133
140. Miyake T, Nakamura K, Arita R, Imada M (2010) Comparison of ab initio low-energy models for LaFePO, LaFeAsO, BaFe2As2, LiFeAs. FeSe and FeTe: electron correlation and covalency. J Phys Soc Jpn 79:044705
141. Miyake T, Pourovskii L, Vildosola V, Biermann S, Georges A (2008) d- and f-orbital correlations in the REFeAsO compounds. J Phys Soc Jpn 77(C):99
142. Miyake T, Pourovskii L, Vildosola V, Biermann S, Georges A (2008) Importance of electronic correlations for structural and magnetic properties of the iron pnictide superconductor LaFeAsO. J Phys Soc Jap C 77:99
143. Nakamura K, Arita R, Imada M (2008) Ab initio derivation of low-energy model for iron-based superconductors LaFeAsO and LaFePO. J Phys Soc Jpn 77:093711
144. Solovyev IV, Imada M (2005) Screening of Coulomb interactions in transition metals. Phys Rev B 71(4):045103
145. Şaşıoğlu E, Friedrich C, Blügel S (2011) Effective Coulomb interaction in transition metals from constrained random-phase approximation. Phys Rev B 83(12):121101
146. Casula M, Werner P, Vaugier L, Aryasetiawan F, Miyake T, Millis AJ, Biermann S (2012) Low-energy models for correlated materials: bandwidth renormalization from coulombic screening. Phys Rev Lett 109:126408
147. Casula M, Rubtsov A, Biermann S (2012) Dynamical screening effects in correlated materials: plasmon satellites and spectral weight transfers from a Green's function ansatz to extended dynamical mean field theory. Phys Rev B 85:035115
148. Tomczak JM, Casula M, Miyake T, Aryasetiawan F, Biermann S (2012) Combined GW and dynamical mean field theory: dynamical screening effects in transition metal oxides. EPL 100:67001
149. Huang L, Wang Y (2012) Dynamical screening in strongly correlated $SrVO_3$. Europhys Lett 99:67003
150. Aryasetiawan F, Biermann S, Georges A (2004) A first principles scheme for calculating the electronic structure of strongly correlated materials: GW+DMFT. Proceedings of the conference "Coincidence Studies of Surfaces, Thin Films and Nanostructures", Ringberg Castle, Sept 2003
151. Biermann S, Aryasetiawan F, Georges A (2003) First-principles approach to the electronic structure of strongly correlated systems: combining the *gw* approximation and dynamical mean-field theory. Phys Rev Lett 90:086402
152. Biermann S, Aryasetiawan F, Georges A (2004) Electronic structure of strongly correlated materials: towards a first principles scheme. Proceedings of the NATO Advanced Research Workshop on "Physics of Spin in Solids: Materials, Methods, and Applications" in Baku, Azerbaijan, Oct 2003. NATO Science Series II, Kluwer, Dordrecht
153. Hansmann P, Ayral T, Vaugier L, Werner P, Biermann S (2013) Long-range Coulomb interactions in surface systems: a first-principles description within self-consistently combined *GW* and dynamical mean-field theory. Phys Rev Lett 110:166401
154. Ayral T, Biermann S, Werner P (2013) Screening and nonlocal correlations in the extended Hubbard model from self-consistent combined *gw* and dynamical mean field theory. Phys Rev B 87:125149
155. Ayral T, Werner P, Biermann S (2012) Spectral properties of correlated materials: local vertex and nonlocal two-particle correlations from combined *gw* and dynamical mean field theory. Phys Rev Lett 109:226401
156. Biermann S (2014) Dynamical screening effects in correlated electron materials – a progress report on combined many-body perturbation and dynamical mean field theory: "GW +DMFT". J Phys Condens Matt
157. Hedin L, Lundqvist S (1969) Solid state physics, vol 23. Academic, New York